ANALYSIS OF BROADBAND HIGH-IMPEDANCE GROUND PLANE ANTENNA DESIGNS

THESIS

James W. Stewart, Captain, USAF

AFIT/GE/ENG/03-17

DEPARTMENT OF THE AIR FORCE

AIR UNIVERSITY

AIR FORCE INSTITUTE OF TECHNOLOGY

Wright-Patterson Air Force Base, Ohio

The views expressed in this thesis are those of the author and do not reflect the official policy or position of the United States Air Force, Department of Defense, or the United States Government.

AFIT/GE/ENG/03-17

ANALYSIS OF BROADBAND HIGH-IMPEDANCE GROUND PLANE ANTENNA DESIGNS

THESIS

Presented to the Faculty

Department of Electrical and Computer Engineering

Graduate School of Engineering and Management

Air Force Institute of Technology

Air University

Air Education and Training Command

In Partial Fulfillment of the Requirements for the

Degree of Master of Science in Electrical Engineering

James W. Stewart, BS

Captain, USAF

March, 2003

AFIT/GE/ENG/03-17

ANALYSIS OF BROADBAND HIGH-IMPEDANCE GROUND PLANE ANTENNA DESIGNS

James W. Stewart, BS

Captain, USAF

Approved:

William D. Wood (Chairman)	10 Mar 03 date
Andrew J. Terzuoli (Member)	10 Mar 2003 date
Gary A. Thiele (Member)	11 Mar '03 date

Acknowledgements

I would like to thank everyone who helped me complete this "independent" research. Foremost is my thesis advisor Major William Wood (AFIT/ENG) for allowing me to continually discuss and pursue new ideas, while ensuring that I was not given too much rope. I also wish to recognize my sponsor, Dr. Dan Janning, and committee members, Dr. Andrew Terzuoli and Dr. Gary Thiele, for their guidance, support, and patience.

I am forever indebted to Mr. Charlie McNeeley (AFIT/ENG) for providing unrestricted access to the radar cross section and antenna chambers as well as fabrication equipment and supplies. I am also indebted to Dr. Leo Kempel for providing his computational electromagnetics software and plenty of guidance to go along with it.

To Keven Golla and Ben Wilmhoff, thanks for laying out the ground work for my research and for patiently addressing each and every one of my questions concerning your research.

Further recognition goes to Rogers Corporation and Wright State University (WSU). The folks at Rogers were very responsive in sending free samples to support my work, and provided a wealth of information concerning materials science and fabrication techniques. On the same note, I am thankful for the unlimited access to the chemical etching laboratory at WSU. To Dr. Ron Reicher (AFRL/SNRR, WSU), your technical expertise and enjoyment in the antenna fabrication and testing process kept me motivated during my research.

Most importantly, my deepest appreciation goes to my wife. Her strong support of my never ending goals, despite enduring many sacrifices along the way, is the leading factor behind every success I've [we've] ever had. To my children, I'm back!

James W. Stewart

Table of Contents

Page

List of Figures

List of Tables

Abstract

This research ties together computational and experimental analysis of two types of high-impedance ground plane (HIGP) antennas. One type of antenna consists of a proposed two-layer design. The structure consists of a bowtie antenna mounted over the surface of a HIGP. The proposed structure was intended to achieve a resonant frequency of 3 GHz and a bandwidth of 48%; however, a design error results in a significant mismatch in operating bands between the antenna and HIGP. Experimental results indicate the structure performs poorly across the entire measured band of 2-5 GHz. A new two-layer design is developed and presented. The new design takes advantage of lessons learned such as designing around material properties of readily available materials.

Analysis of integrated, or one-layer, HIGP antennas are also presented. The one-layer versions utilize the exact same design parameters as their corresponding two-layer designs; the bowtie radiating element is simply positioned in the plane of, rather than over, the HIGP. Results indicate the design error in the proposed two-layer structure affects the performance of the one-layer version less than the two-layer antenna. A comparison between the original and new integrated HIGP antennas show an improvement in input impedance, but a decrease in bandwidth.

ANALYSIS OF BROADBAND HIGH-IMPEDANCE GROUND PLANE ANTENNA DESIGNS

I. Introduction

Aircraft antennas are instrumental in supporting airborne missions. The functional requirement of any antenna, whether land, sea, or air based, is to effectively transmit and/or receive electromagnetic energy between distant locations. Yet each type of antenna has its own set of design constraints. Since the birth of wireless, land based antennas of all shapes and sizes have been developed to effectively transfer energy between distant points. Some are relatively simple, such as the common dipole antenna found on an AM radio. Others are quite extravagant–and expensive–such as the 305-meter spherical reflector at the Arecibo Observatory in Puerto Rico. On the other hand, airborne antenna designs have much less flexibility in size, weight, and often in cost. Furthermore, in many applications such as communication, navigation, remote sensing, etc..., an antenna must effectively operate over a wide frequency band. Like land based antennas, many types of airborne antennas exists that satisfy their intended tasks. The High-Impedance Ground Plane (HIGP) enhanced antenna is one type of design that satisfies many current airborne antenna requirements, and perhaps more importantly, may satisfy more demanding requirements of future platforms. The HIGP antenna is compact, relatively light, inexpensive, and may be ideal for low observable (LO) aircraft.

1.1 Background

In the development of modern aircraft, the Air Force puts increasingly more stringent requirements on LO designs. In other words, aircraft must be less detectable by radar, optical, and acoustic sensors. Much effort is put into reducing the radar cross section (RCS) of a platform. Knott defines RCS of a system [target] as "the projected area of a metal sphere that would scatter the same amount of power in the same direction that the target does" [6]. An important point is that a system's RCS is the one parameter in the radar detection process that an LO engineer may influence. One method of reducing RCS is to minimize the number of structures protruding from an aircraft, i.e., storing bombs and missiles inside an aircraft rather than on its wings. The same principle can be applied to the design of antennas. The HIGP antenna may be an ideal solution for LO antenna designs. In 1998, Sievenpiper introduced the HIGP as a novel structure that behaves like a perfect magnetic conductor (PMC) in the radio frequency (RF) spectrum [14]. The HIGP concept is an extension of the photonic band-gap (PBG) concept introduced by Yablonovitch in 1987 [20]. The HIGP exhibits two characteristics that may lead to a LO antenna design:

1. The HIGP reflects electromagnetic waves in phase with incoming waves.
2. The structure does not support surface traveling waves.

Since it reflects waves in phase with incoming waves, the HIGP can be designed as a conformal antenna, i.e., it can be flush with, rather than protruding from, the surface of an aircraft. Conformal designs reduce RCS. Unlike existing conformal antennas such as cavity-backed antennas, the HIGP may benefit from additional RCS reduction due to its ability to suppress surface traveling waves. Surface traveling waves are waves that travel along a metal surface and scatter (radiate) from its edges. This undesirable phenomenon not only degrades the performance of antennas, but also adds to their RCS. Although they may provide new opportunities in the design of LO antennas, current HIGP structures have some barriers to overcome.

1.2 Problem Statement

The HIGP antenna has two characteristics that prevent its use in many applications. First, the antenna has a narrow bandwidth. In this report, bandwidth is defined as the frequency range over which an antenna efficiently operates i.e. the range that the voltage standing wave ratio (VSWR) of the antenna is 2:1 or less. Sievenpiper's original design exhibited a bandwidth of 5%. Current designs have stated bandwidths on the order of 10% to 20%. Narrow band antennas are satisfactory for many airborne applications, but some systems require large bandwidths. In fact, some systems, such as communications, navigation, and radar systems, require an antenna with a bandwidth greater than 100%. Second, predictions from numerical modeling often do not agree with measurements of actual HIGP antennas. Modeling is especially inaccurate in the prediction of the antenna's bandwidth [15]. Although it can rely solely on prototype testing, the antenna design process is less time consuming and costly with the aid of accurate computer modeling. If these shortcomings can be resolved, the HIGP may be an ideal solution for many Air Force applications.

This thesis is a continuation of a two-layer HIGP antenna design proposed by Wilmhoff [18]. The design has neither been tested through experimental, nor computational means. It is based on a HIGP designed to resonate at 3 GHz with a bandwidth of 48%, and a broadband radiating element designed for a center frequency of 3 GHz. One potential and one known problem are explored. First, the proposed antenna is based solely on design equations–it is not supported by any type of analysis. Second, a deficiency exists in the modeling process which prevents computational modeling of the antenna structure [19]. As described during an interview with Wilmhoff, the HIGP and antenna structures can be modeled separately, but software limitations prevent modeling the integrated structure. This deficiency prevents analyzing the near field effects, or mutual coupling between the two layers.

1.3 Research Goal

The Wilmhoff design may lead to a successful broadband HIGP antenna, but time constraints ended his research. The primary goal of this research is to evaluate the proposed broadband HIGP antenna. Success is based not only on the extent of experimental and computational results obtained, but also on the correlation in results between the two methods.

1.4 Assumptions

Two categories of assumptions exist in this thesis. Several derivations include assumptions inherited from cited references, i.e., in equations developed by other authors. Additional assumptions made in this research are the following:

1. Dielectric materials are lossless, linear, homogeneous, isotropic, and nondispersive.
2. Metals are perfect electric conductors.
3. Transmission lines have a characteristic impedance of 50 Ω.

Within the measured frequency bands in the research, the substrate materials selected for the prototypes are designed to exhibit the dielectric approximations listed. The metallic structures of the prototypes are either copper or aluminum. Both type of metals have conductivities that allow for a reasonable approximation as perfect electric conductors. In addition, the measurement equipment and computational methods are designed to exhibit a 50 Ω characteristic impedance.

1.5 Scope

The primary objective of this research is to demonstrate a HIGP antenna operating over a wide frequency band. The development of the antenna prototype is based on the antenna design presented in Wilmhoff's thesis. The antenna has the following expected parameters: center frequency of 3 GHz and bandwidth of 48%. One of the main tasks of this thesis includes developing a work-around for a software deficiency. The meshing

software must allow evaluation of the entire structure as a whole. Computational modeling must closely match the prototype for a valid comparison of results. A secondary goal is to develop a one layer version of the antenna–placing the antenna in the plane of the HIGP. This one-layer concept as presented by Golla [4] simplifies the fabrication process and reduces costs. The primary figure of merit of each antenna is the 2:1 VSWR bandwidth, or -9.5 dB return loss, depending on the particular measurements involved.

1.6 Resources

This research utilizes computational resources, fabrication materials and equipment, and measurement equipment. Specific requirements include:

1. High performance computing capability.
2. A FORTRAN 90 Compiler, CADStd ©, MATLAB ©, Dfx2xyz ©, SkyMesh2 ©, WIPL- D © and Prism software packages.
3. Milling and chemical etching equipment along with associated supplies.
4. Printed circuit board (PCB) and coaxial feed materials.
5. A network analyzer, antenna test range, and RCS test range.

1.7 Overview

This thesis presents theories related to the HIGP, methodologies in evaluating their designs, RCS analysis, and finally experimental and computational results of several HIGP antennas. Chapter II provides a literature review focusing on bandwidth and computational methods. An in-depth RCS analysis of a HIGP as a reflector is presented in Chapter III. Chapter IV describes the methodology used in testing and evaluating HIGP antenna designs. Chapter V presents results and analysis of tested antenna designs. Finally, a brief set of conclusions and recommendations for future research is presented in Chapter VI.

II. Literature Review

In 1998, Sievenpiper introduced the HIGP as a novel structure that behaves like a perfect magnetic conductor (PMC) in the radio frequency (RF) spectrum [14]. The HIGP concept is an extension of the photonic band-gap (PBG) concept introduced within the physics community in 1987 [20]. Many articles in fact refer to the HIGP as a PBG structure. Although it provided new opportunities in the design of electromagnetic devices, the HIGP structure had two characteristics that prevented usage in many applications:

1. The structure exhibited a narrow bandwidth.
2. Computational modeling was unable to predict the bandwidth [15].

By resolving these shortcomings, the HIGP may be an ideal solution for many Air Force applications.

Over the past five years, variations of HIGP structures have emerged. Several of these are examined with the following questions in mind: which design provides the largest bandwidth; which numerical technique best predicts measured bandwidth results. Before comparing various designs, a derivation of the HIGP surface model may provide a basis for evaluation.

2.1 The High Impedance Surface Model

Two material modeling techniques are used in the derivation of the HIGP. The effective reflection plane (ERP) method is used to define its reflective wave behavior. The phase of the reflective wave, as seen in the far field, is compared to that of a PEC reference plane. Using the phase comparison, the effective bandwidth is defined as the frequency band between the -90° and 90° phase difference. Referring to Figure 1, a representative HIGP reflection measurement may contain a 360° phase reversal over an extended frequency band. On the other hand, the reflection from a PEC surface is a constant -180°.

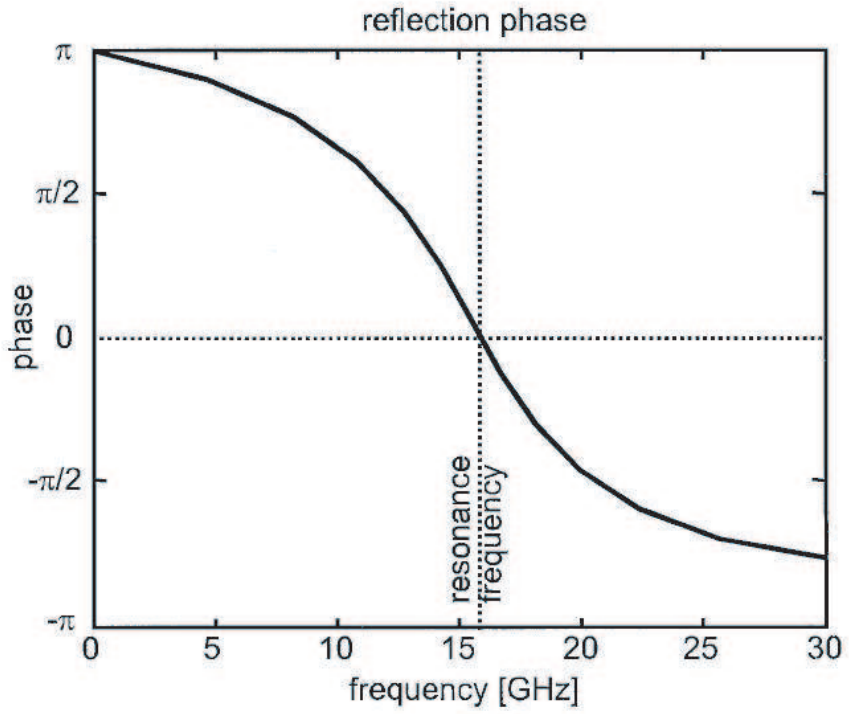

Figure 1 Reflection phase of a HIGP with a resonant frequency of 15 GHz, and an effective operating band from 10 GHz to 20 GHz, Sievenpiper [15].

The effective medium model is another technique used to describe a HIGP. The model enables a derivation of the effective permittivity of a ground plane. Sheet capacitance can then be derived through conformal mapping techniques. In his dissertation [14], Sievenpiper utilizes the effective medium and ERP models to develop properties of a high impedance ground plane, see Figure 2.

The resonant frequency and bandwidth are derived from the effective sheet inductive and capacitive properties, which themselves are derived through conformal mapping of the electromagnetic properties and geometry of the structure.

Sievenpiper used circuit theory to develop fundamental properties of the HIGP. As shown in the parallel circuit model in Figure 3, the inductance is only a function distance

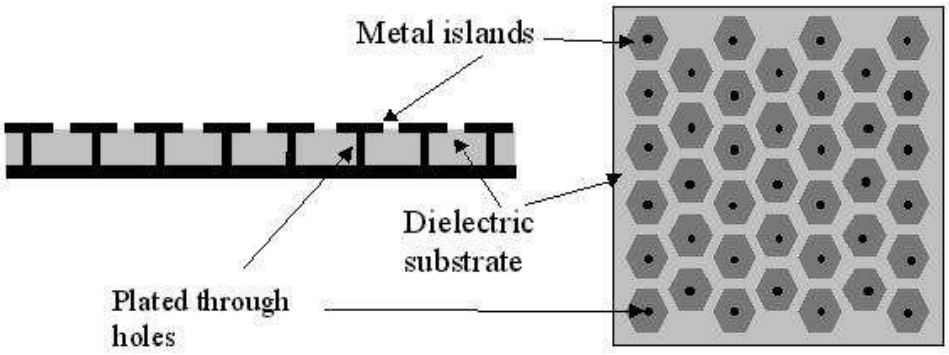

Figure 2 "Thumbtack" high-impedance ground plane geometry, Sievenpiper [15].

between the surface and ground plane given by

$$L = \mu_r \mu_0 t \ (\textit{Henrys/square}) \tag{1}$$

where L is the sheet effective inductance, μ_r is the relative permeability of the dielectric material, μ_0 is the permeability of free space, and t is the substrate thickness.

The capacitance of individual elements is a function of both the surface geometry and the material properties given by

$$Ce = \frac{w(\varepsilon_1 + \varepsilon_2)}{\pi} \cosh^{-1}\left(\frac{a}{g}\right) \ (\textit{Farads}) \tag{2}$$

where Ce is the capacitance of an individual element, w is the edge length of an element, ε_1 is the permittivity of a free space, ε_2 is the permittivity of the substrate, g is the gap between elements, and a is the center-to-center spacing between the vias, see Figure 4.

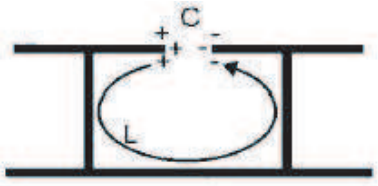

Figure 3 Parallel circuit model of thumbtack design.

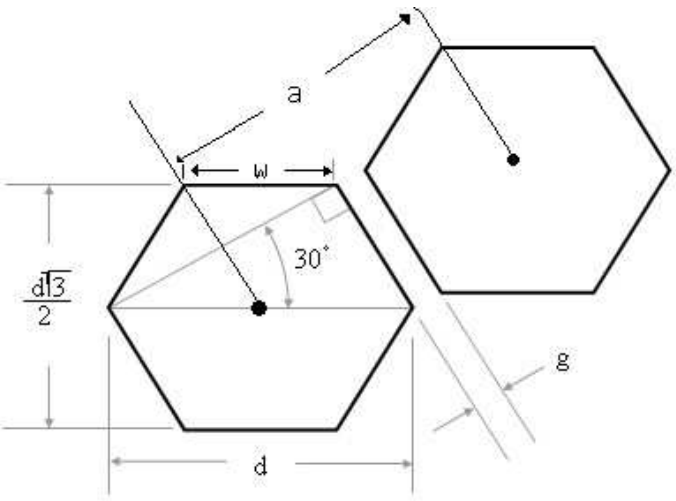

Figure 4 HIGP Element Design Parameters.

Sheet capacitance is then obtained by multiplying the individual element capacitance by a scaling factor given by

$$C = Ce \times F\,(Farads/square) \tag{3}$$

where C is the sheet capacitance, and F is a factor determined by the geometry of the HIGP elements.

Sievenpiper provides the scaling factor of square, hexagonal, and triangular elements as equal to 1, $1/\sqrt{3}$, and $\sqrt{3}$ respectively. Using circuit theory, the surface impedance of the parallel LC circuit model is

$$Z = \frac{j\omega L}{1 - \omega^2 LC} \tag{4}$$

where Z is the surface impedance, ω is the frequency in rad/sec, and L and C are the sheet inductance and capacitance respectively. Again using circuit theory, the resonant frequency, ω_0 occurs at

$$\omega_0 = \frac{1}{\sqrt{LC}} \tag{5}$$

which causes $|Z| \rightarrow \infty$ ("High Impedance"). Finally, Sievenpiper derives the HIGP ERP based bandwidth as

$$BW = \sqrt{\frac{\mu_r}{\varepsilon_r}} \cdot \frac{t}{w} \tag{6}$$

Choosing a material with a relative permeability of one and integrating an existing antenna (i.e., w is predetermined,) leaves only two variables (ε_r and t) in the bandwidth design.

2.2 HIGP Bandwidth Design

Armed with Equations (5) and (6), one may idealistically design a HIGP of great bandwidth centered about any desired frequency; however, an examination of several designs proves otherwise.

Early in his research, Sievenpiper achieved a bandwidth of 5.4% for an antenna operating at 14.75 GHz [10]. His prototype was constructed on a dielectric with a relative permittivity of 10.2 and thickness of 25 mils (1 mil = 0.001 inches). Although the prototype's bandwidth is three times wider than that of a conventional patch antenna, it remains unusable for wideband applications.

Coccioli achieved antenna designs with predicted bandwidths of 21.3% and 11.5% using Finite Difference Time Domain (FDTD) modeling [3]. A bandwidth of 11% is a benchmark in HIGP design; a bandwidth of 21% would represent a significant advance in HIGP technology. Unfortunately, only the 11% bandwidth design is demonstrated through experimental means. In addition, Coccioli's HIGP measured results do not match the predicted values. His variation of the HIGP, termed a uni-planar compact photonic bandgap (UC-PBG), is based on a dielectric of high permittivity (ε_r = 10.2) and thickness of 25 and 50 mils respectively for the 21% and 11% bandwidth designs. Contrary to Sievenpiper's HIGP design, Coccioli's design provides a bandwidth that decreases with an increase in dielectric thickness. Some recent designs do not result in such advances, but rather decrease HIGP performance-at least from the perspective of bandwidth.

Ali proposed a HIGP patch antenna that provides a 60% increase in bandwidth over a conventional patch antenna [1]. The design utilizes a dielectric with a relative permittivity of 3.38 and thickness of 59 mils. Numerical results indicate the relative increase in bandwidth of 60%; however, conventional patch antennas have very narrow bandwidths-on the order of 1.2%. The proposed HIGP design provides a restrictive 2.8% bandwidth. On the other hand, a small bandwidth is not necessarily the result of an ineffective design.

Salonen, Keskilammi, and Sydanheimo demonstrate a low cost PBG patch antenna that extends the bandwidth of a conventional patch antenna by a factor of three [12]. The resulting PBG antenna has only a 100 MHz bandwidth centered at 2.45 GHz, but this 4.7% bandwidth covers 100% of its intended operating band. The design uses a 59 mil thick FR-4 substrate with a dielectric constant of 4.9. Unfortunately, although the antenna meets its intended bandwidth specifications, an evaluation of the design method cannot be accomplished due to a lack of information. Neither analytic derivation nor numeric predictions are provided.

Along the same lines, Golla provides extensive experimental research into broadband HIGP designs [4]. Several different designs incorporating a printed log-periodic dipole over a HIGP were fabricated and tested. The goal was to design a HIGP bandwidth to accommodate the 2 to 18 GHz operational band of the log-periodic antenna. One design did perform well when limited to receive mode. One of the most interesting outcomes of the research is what Golla refers to as an integral antenna design, see Figure 5. The concept is to integrate an antenna structure into the plane of the HIGP surface, rather than over the surface. A version of this one-layer is presented in Chapter V of this thesis.

In an age where antenna design relies heavily on computer modeling, measurements by themselves are not enough. Accurate numerical methods reduce the amount of time and cost of the design process.

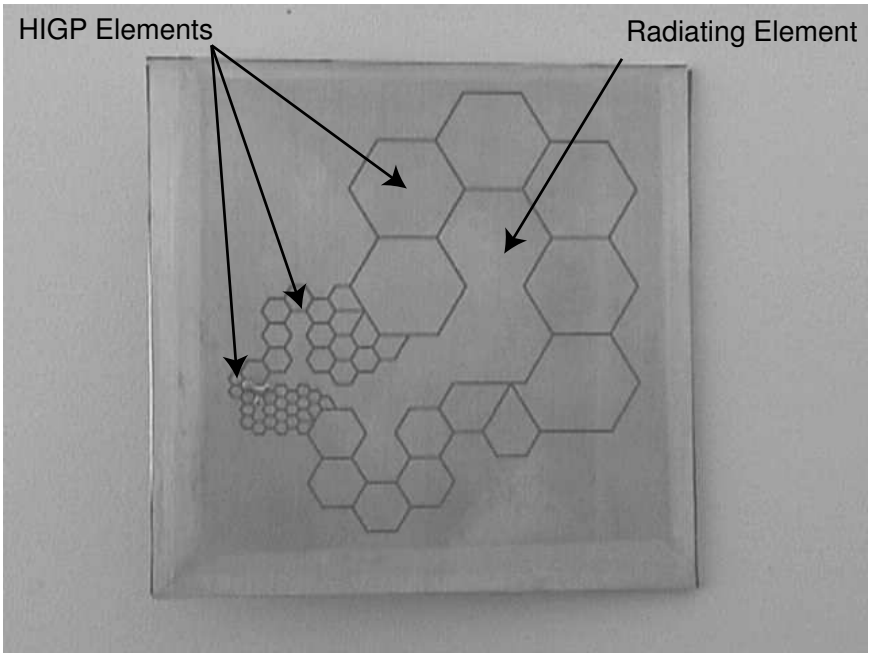

Figure 5 One-arm of a log-periodic antenna integrated into a HIGP [4].

2.3 Numerical Evaluation

In one of the most frequently cited HIGP articles [15], Sievenpiper *et al* presents a detailed analysis of his original HIGP design. Results of computer modeling, using the Finite Element Model (FEM), validate the design. The modeling predictions compare very well with both analytic and measured results in all but one area. Sievenpiper points out that the numerical result "does not predict an actual band-gap" [15]. The authors resort to predicting bandwidths indirectly by extrapolating phase data with measured bandwidth results. Since the FEM numerical method does not allow direct predictions of bandwidth, other techniques must be explored.

In another article [10], Sievenpiper refers to FDTD in modeling his HIGP. He points out that FDTD was used in optimizing the antenna design but does not mention how well predicted values of bandwidth compare to measured results. More than one paper has prevented the evaluation of numerical modeling by either focusing solely on the modeling itself, or just on the measured results.

A design exhibiting a bandwidth of 20% was developed by Rahman and Stuchly [11]. Again, FDTD was used in optimizing the antenna structure. In this case, no prototype was constructed, and therefore, no comparison of measured results is possible.

Ali used a FEM based program, High Frequency Structure Simulator (HFSS), to model his HIGP antenna design [1]. He describes the design in great detail, but does not include any measured results of the prototype. Numerical results alone do not enable evaluation of his HFSS model; a comparison of measured versus predicted results is necessary for proper validation. Others have produced large amounts of both predicted and measured data, but with disagreements between the two.

During his thesis work [18], Wilmhoff utilized a custom FEM code developed at Michigan State University to model an HIGP antenna design. Interestingly, the code (Prism) does not correctly predict the measured bandwidth of the integrated HIGP antenna structure; however, it accurately predicts the bandwidths of the antenna and HIGP structures individually. In a personal interview [19], Wilmhoff explained the inability of Prism to model complex multi-layered structures. He suggests using separate modeling programs to optimize the antenna and HIGP structures separately, then use Prism to run simulations of the integrated structure. This is the modeling approach used within this thesis.

2.4 Conclusion

This review examined several different HIGP antennas that increase antenna bandwidth. Demonstrating a bandwidth of 10%, Coccioli's UC-PBG design clearly achieves best results [3]. In addition, he models a design having a 20% bandwidth. If successfully developed, Coccioli will achieve a great breakthrough in HIGP antenna design. Sievenpiper achieves a bandwidth of 5% during a follow-on effort to his original design [10]. Although the bandwidth is on the same order as the original HIGP, he achieves greater power gain from the antenna. Recent designs by Ali [1], and Salonen [12] also achieve bandwidths on the same order as Sievenpiper's original HIGP antenna. After examining

all four designs, Coccioli's UC-PBG design demonstrates the largest bandwidth of HIGP antennas. Can these designs be accurately modeled?

The question as to which numerical technique best predicts measured bandwidth of an HIGP antenna is not clearly answered. Five modeling examples were examined. Versions of FDTD [10, 11] and FEM [1, 15, 18], were used in modeling the antennas. In both cases of the FDTD modeling, predicted values are not compared to measured results thus the accuracy of FDTD modeling cannot be evaluated. Along the same lines, the HFSS simulations are not compared with measured data. On the other hand, two cases involving the FEM code are backed with adequate measured data. During Sievenpiper's research, the predictions from FEM compared well with all measured data but was unable to directly predict a bandwidth value [15]. The method lacks the ability to predict the very parameter that this research is focused on. The version of FEM code used by Wilmhoff also demonstrated some limitation in modeling an HIGP antenna. The limitations in this case involved more than just bandwidth predictions. In fact, Wilmhoff suggests using other modeling processes to supplement the FEM based modeling. Of the five cases, the FEM modeling code appears to be the most accurate numerical technique. Its limitations are known and may be overcome by modifying, or supplementing, the code.

III. Radar Cross Section Characterization

Chapter II provided insight into attainable bandwidths of high impedance ground planes. Chapters IV and V develop methodology and provide results of HIGP antenna designs intended to set a new benchmark in bandwidth. This chapter characterizes a HIGP design as a PMC reflector. Scattering analysis is used to compare the traveling wave suppression and radar cross section (RCS) reduction capability to those of known targets.

3.1 Introduction and Objectives

A square perfect electric conducting (PEC) plate can have significant RCS contributions from surface traveling waves. A key feature of a HIGP is its theoretical ability to suppress such traveling waves. Consequently, a HIGP may have a lower RCS than a PEC ground plane of the same dimensions. The objective of this chapter is to characterize the HIGP's impact on RCS as follows:

1. Does the HIGP completely suppress surface waves at its resonant frequency?
2. Does the HIGP suppress surface waves at its cut-off frequencies?
3. What impact on RCS does the HIGP have relative to an equivalent PEC plate?
4. Does the HIGP alter scattering parameters such as beamwidth and side lobe levels?

The Air Force Institute of Technology's RCS range is used to observe and measure the RCS of a HIGP and a magnetic radar absorbing material (RAM) treated aluminum plate. The HIGP is constructed using a hexagonal element pattern described in chapter II. The second target contains RAM on only one surface. The opposite surface (aluminum) provides a PEC reference plate. The targets are measured at different aspect angles (pattern cuts), and frequencies (frequency sweeps). The pattern cuts are measured at the HIGP resonant frequency, and lower and upper cut-off frequencies of 13.2, 10.5, and 16.0 GHz respectively. Frequency sweeps are conducted at normal incidence and traveling wave peak gazing angles relative to the resonant and cut-off frequencies.

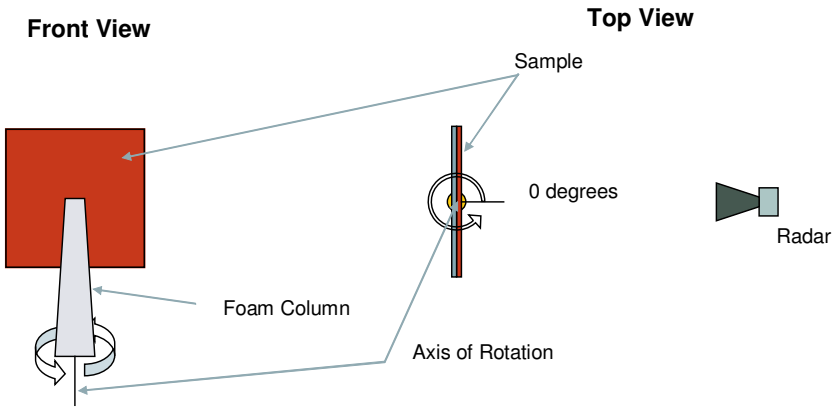

Figure 6 Target orientation for RCS measurements.

3.2 Procedures and Setup

AFIT operates an indoor RCS range facility. The range is an open-air, direct illumination facility with a frequency range of 6.2-18.2 GHz. Dimensions of the anechoic chamber are approximately $45' \times 24' \times 26'$ with a tapered ogive pedestal in the center. The horn antenna and target center are 27' apart, both at a centerline height of eight feet above the floor, see Figure 6 for target orientation. The range uses a Lintek 4000 system. The radar and the target pedestal are computer driven via a Mission Research Corporation (MRC) software graphical user interface. The software allows automated control of frequency, angle and polarization configurations for each measurement.

3.2.1 Test Items. Test items include two $6" \times 6"$ flat plates, see Figure 7. The HIGP is constructed on a 59 mil (1.499 mm) thick FR-4 substrate and based on a hexagonal element design, see Table 1 for list of design parameters. Using the values in Table 1 for Equations (5) and (6) in Section 2.1, the HIGP has a nominal resonant frequency of 13.2 GHz and bandwidth of 41.5%. Its surface contains two defects (cavities) were hex elements where removed. The cavities are 0.15" in diameter and located 1" from upper left corner of the HIGP as viewed broadside.

(a) Target 1 front. (b) Target 1 back. (c) Target 2 front. (d) Target 2 back.

Figure 7 Test targets: Target 1, (a) HIGP front, (b) copper back; Target 2, (c) RAM front, (d) Aluminum back.

Table 1 HIGP Target Design Parameters.

Parameter	Symbol	Value
Substrate thickness	t	1.499 mm
Relative Permittivity	ε_r	4.9
Element Edge Length	w	1.524 mm
Element Spacing	g	0.254 mm
Via Spacing	a	2.640 mm
Correction Factor	F	$1/\sqrt{3}$

Data on the RAM performance is limited. The only specification known is that it provides a 10 dB power reduction at normal incidence over the 4 to 10 GHz band. Although most of the tests are conducted at frequencies above 10 GHz and angles other than broadside, a -10 dB value is used in each test configuration to estimate the RAM reduction.

3.2.2 Test Procedures. The targets were tested according to the test matrix shown in Table 2. All tests were performed in horizontal polarization. Each tests included background clutter measurements to account for RCS from: chamber and pedestal hardware, target and calibration mounts (styrofoam), and calibration target. The calibration target is a 6" diameter sphere. The measured coherent data, proportional to the back-

catter power, was combined with the calibration target's theoretical solution through the following

$$\sigma_{cal} = \frac{\sigma_{tgt} - \sigma_{tgt.bck}}{\sigma_{cal.tgt} - \sigma_{cal.tgt.bck}} \sigma_{thy} \tag{7}$$

where σ_{tgt} is the target data, $\sigma_{tgt.bck}$ is the target background data, $\sigma_{cal.tgt.bck}$ is the calibration background measurement, and $\sigma_{cal.tgt}$ and σ_{thy} are the measured and theoretical values of the 6" sphere calibration sphere.

Table 2 RCS Test Matrix.

Target[1]	F [GHz]	Az [deg.][2]
1	10.5	0-360
1	13.2	0-360
1	16.0	0-360
2	10.5	0-360
2	13.2	0-360
2	16.0	0-360
HIGP	6.2-18.2	0.0
HIGP	6.2-18.2	17.2
HIGP	6.2-18.2	18.9
HIGP	6.2-18.2	21.2
RAM	6.2-18.2	0.0
RAM	6.2-18.2	17.2
RAM	6.2-18.2	18.9
RAM	6.2-18.2	21.2
PEC	6.2-18.2	0.0
PEC	6.2-18.2	17.2
PEC	6.2-18.2	18.9
PEC	6.2-18.2	21.2

All target, background, and calibration measurements were completed within a short time of each other to minimize error associated with radar "drift" or thermal interference. In addition, background and calibration data were collected for each combination of frequency and polarization in the test matrix.

[1] All target measurements conducted in horizontal polarization.
[2] Azimuth of 0° represents target broadside.

Finally, an accurate target RCS was obtained through post processing. All measured data for each configuration was read into the MRC Software, which corrects the target data using Equation (7) and generates plots.

3.3 Predicted Values

Knott *et al* provide "hip pocket" formulas enabling accurate RCS predictions for simple targets [6]. The calculations depend only on target geometry and incident wavelength. Where appropriate, a 10 dB reduction from RAM is incorporated into the formulas. Using a constant 10 dB reduction for all frequencies and angles introduces errors, but simplifies the predictions in the spirit of "hip pocket" formulas.

The first consideration is the presence of traveling waves. The peak grazing angle at which such waves occur is given by

$$\theta_{pk-tw} = 49\sqrt{\frac{\lambda}{L}} \tag{8}$$

where θ is the grazing angle in degrees, λ is the incident wavelength, and L is the physical side length in meters. The surface traveling wave RCS magnitude is no greater than:

$$\sigma_{pk-tw} \leq 3\lambda^2 \tag{9}$$

Estimates for the specular RCS are provided by

$$\sigma_{PEC} = 4\pi \left(\frac{Area^2}{\lambda^2} \right) \tag{10}$$

$$\sigma_{RAM} = 10\log_{10}(\sigma_{PEC}) - 10dB \tag{11}$$

where σ_{PEC}, and σ_{RAM} represent specular RCS of the PEC plate, and RAM coated plate respectively. The specular RCS of HIGP plate is not predicted as it contains a textured surface of metal and dielectric. Additional values of interest include the edge diffraction and beamwidth. In reference to Figure 6, edge diffraction occurs during horizontal

polarization and is predicted as

$$\sigma_{edge} = \frac{L^2}{\pi} \tag{12}$$

where *L* is the physical edge length in meters. Finally, the approximate scattered beamwidth is given by

$$BW_{null-to-null} = 57\frac{\lambda}{L} \tag{13}$$

where *BW* is beamwidth in degrees. All predicted values, along with measured results, are listed in Tables 3 and 4 in Section 3.4.

3.4 Results and Analysis

Several observations can be made about the HIGP's ability to reduce traveling waves and RCS. All measurements indicate that the HIGP provided a significant reduction of traveling waves at its resonant frequency. Table 3 provides a summary of the predicted and measured traveling waves for each target. At its resonant frequency, the HIGP had a peak traveling wave of -33 dB. The pattern-cut results show the HIGP provided a 11 dB reduction compared to the PEC plate and a 6 dB reduction compared to the RAM plate, see Figure 8. At its cut-off frequencies, the HIGP had the same peak traveling wave levels as the PEC plate.

Table 3 Predicted and Measured Surface Traveling Wave (TW).

Target	F [GHz]	θ_{pk-tw} [deg.]	σ_{pk-tw}	
			Predicted	Measured
PEC	10.5	21.2	-26.1	-20
PEC	13.2	18.8	-28.1	-22
PEC	16.0	17.2	-29.8	-19
RAM	10.5	21.2	NA	-27
RAM	13.2	18.9	NA	-27
RAM	16.0	17.2	NA	-26
HIGP	10.5	21.2	$<$-26.1	-22
HIGP	13.2	18.9	$\ll$-28.1 [1]	-33
HIGP	16.0	17.2	$<$-29.8	-22

[1] A HIGP theoretically does not support surface traveling waves at its resonant frequency.

As shown in the downrange plots in Figure 9, the HIGP trailing edge return was nearly three times lower than that of the PEC target when the targets were oriented at the expected peak grazing angles. The results are not entirely valid since the downrange plots were based on a broadband measurement. The plots were formed through a discrete Fourier transform (DFT) of a 6-18 GHz frequency sweep measurement of each target. On the other hand, the HIGP has a predicted bandwidth of only 10-16 GHz. The reduction in the far edge return of the HIGP may be lower if measured only within its operating band.

The frequency sweeps alone reveal distinct differences in scattering behavior between the HIGP, PEC, and RAM plates, see Figure 10. The HIGP response consists of a lobing pattern of fairly constant peaks until it reaches its resonance frequency (13.2 GHz). In fact, below its lower cut-off frequency, the HIGP response closely resembles that of the PEC plate. The HIGP may look like a solid plate to long wavelengths–similar to a wire grid antenna. Beyond resonance, the RCS steadily drops–up to 10 dB lower than the RAM treated target in some cases. At frequencies above its cut-off frequency, the HIGP response closely tracks that of the RAM target. One possible explanation for this behavior is that short wavelengths may easily propagate through the HIGP surface gaps and attenuate within the structure, or exit from the sides of the plate. The results also show that the HIGP has a null at its resonant frequency while the PEC and RAM targets have a peak at the same frequency. Since lobing patterns are caused by constructive and destructive interference of edge diffractions, the null may be attributed to the significant reduction of traveling waves when the HIGP is at resonance.

Perhaps most interesting is the fact that the first observed null was very deep for the HIGP. At $18.9°$, the HIGP had a - 40 dB null at about 9 GHz. The RAM had a null of only -27 dB for the same test. The HIGP not only reduced surface waves, but also provided a significant RCS reduction compared to the RAM in some cases. The structure may lend itself to a directional nulling application.

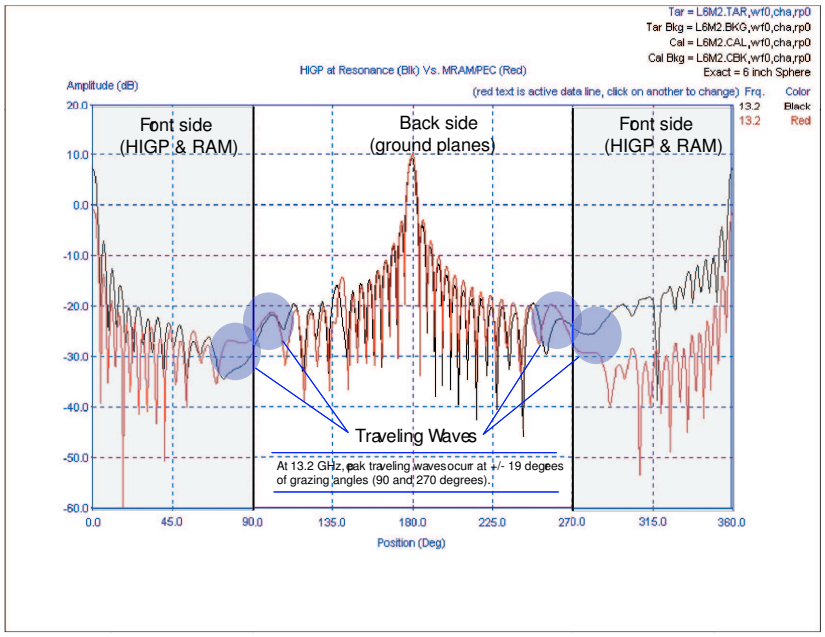

(a) RCS at f_R, 13.2 GHz.

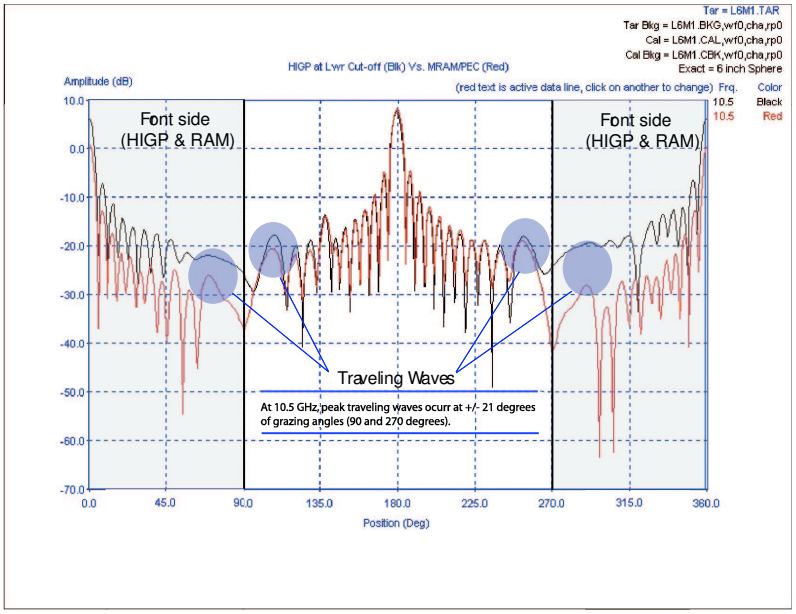

(b) RCS at f_L, 10.5 GHz.

Figure 8 RCS of HIGP (black) vs. RAM/PEC plate (red) at HIGP resonant f_R and lower cut-off frequency f_L. Horizontal polarization used in all measurements.

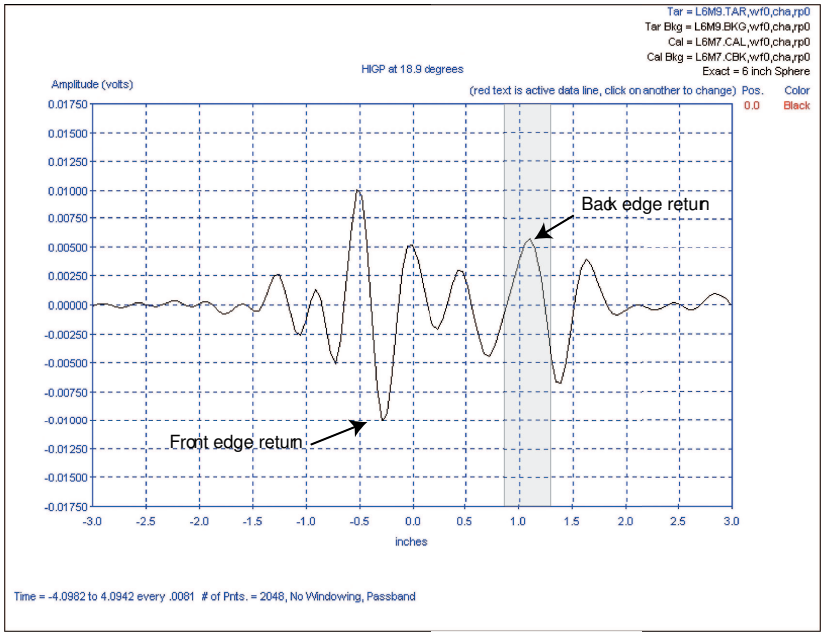

(a) HIGP target return.

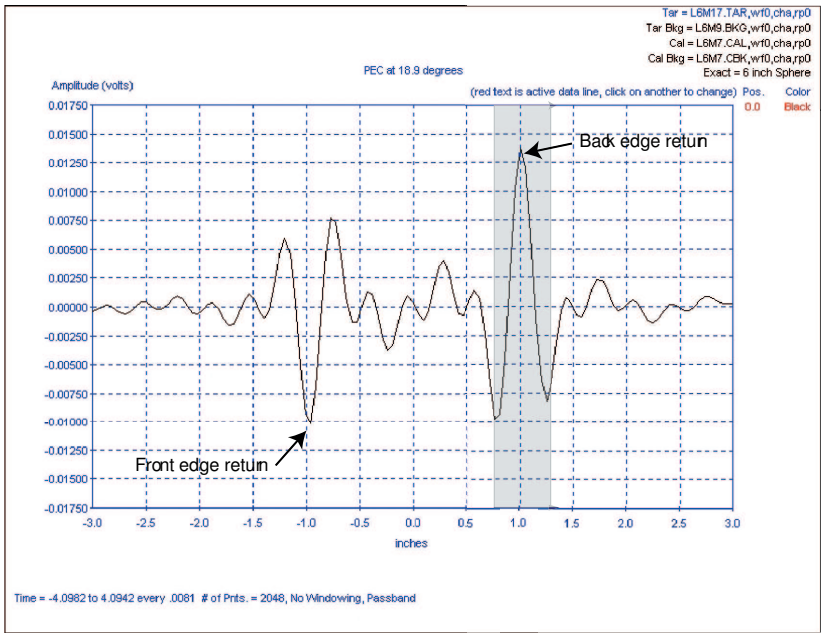

(b) PEC target return.

Figure 9 Down range plots with targets oriented at the predicted peak grazing angle, $\theta = 18.9°$, of the HIGP at resonance. Based on a data collected over the 6-18 GHz band.

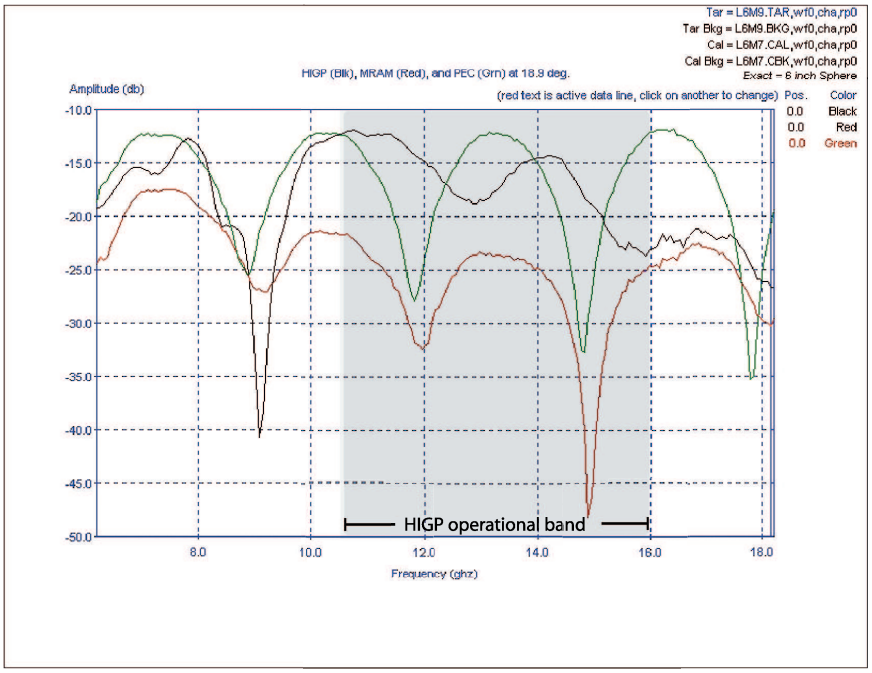

Figure 10 RCS of HIGP (black), PEC (green), and RAM (red) targets at peak grazing angle, θ = 18.9°, for the HIGP resonant frequency f_R = 13.2 GHz.

As shown in Table 4, all measured RCS values were relatively close to their predicted values. The measured broadside RCS values for the PEC plate were within 1 dB of predicted values. The RAM measured values were within 2-4 dB–more accurate at the lower frequencies. As hypothesized, the HIGP RCS values were lower than PEC values–about 2-4 dB lower. Nearly all measured edge-on values were in the -20 to -30 dB range; edge-on values for each target were close to the predicted -21 dB value. No unexpected behavior was observed with beamwidth or side lobe levels of the HIGP.

The individual beam widths (BW) and side lobe levels (SLL) did not appear to vary between targets. Each BW was nearly identical for all three targets at a given frequency and all 1st SLLs were about 13 dB down from peak levels, see Table 4. Unexpected behavior was observed in other areas. Looking at Figure 8, the HIGP RCS was not symmetric about the broadside angle. The HIGP RCS was 3 to 5 dB higher from 270° to 350°

Table 4 Predicted and Measured RCS and Beamwidth (BW).

Target	F [GHz]	$\sigma_{broadside}$ [dBsm]		σ_{edge} [dBsm]	BW [deg]	
		Predicted	Measured	Measured	Predicted	Measured
PEC	10.5	9.2	8.2	-37/-41	10.7	10.6
PEC	13.2	11.2	10.1	-26/-27	8.5	8.5
PEC	16.0	12.9	12.1	-23/-24	7.0	7.0
RAM	10.5	-0.8	0.6	-37/-41	10.5	10.5
RAM	13.2	1.2	-1.0	-26/-27	8.5	8.5
RAM	16.0	2.9	-1.3	-23/-24	7.0	6.5
HIGP	10.5	$<$9.2	6.0	-26/-25	10.7	11.5
HIGP	13.2	$<$11.2	7.2	-29/-24	8.5	9.0
HIGP	16.0	$<$12.9	8.1	-29/-23	7.0	7.0

(1st null) than it was from 10° (1st null) to 90°. The asymmetry was most pronounced at the highest measured frequency. Outside of its bandwidth, the HIGP should behave as a PEC plate. Even if the actual upper cut-off frequency is below the predicted 16.0 GHz, the HIGP should have had a symmetric response about its broadside angle. One possible cause is the defects in the HIGP (two small cavities). They may contribute differently to the RCS depending on the orientation of the HIGP.

One last observation is that all of downrange plots clearly showed edge scattering in the expected locations given by

$$d = L \sin\theta \tag{14}$$

where *d* is the separation between front and back edge returns, *L* is the physical length of the target, and θ is the angle of incidence. Referring to Figure 9, the distance between peaks of the opposite edges is about 1.9" as expected for a 6" target illuminated at angle of 18.9°.

3.5 Conclusion

In conclusion, all measurements clearly indicate the HIGP suppressed, but did not eliminate, surface traveling waves. At its resonant frequency, the structure provided a significant traveling wave reduction compared to a PEC plate of the same dimensions,

but showed no further reduction at its cut-off frequencies. The HIGP also provided RCS reduction compared to a PEC target and in some cases it provided greater RCS reduction than a RAM treated target. At broadside, pattern-cuts indicate an RCS reduction of 2 to 3 dB lower than that of a PEC plate. Results also indicate the HIGP surface had no effect on the beam width and side lode levels. Finally, HIGP surface defects, in the form of cavities, may significantly increase its RCS. Overall results indicate that a HIGP based antenna may be one solution towards an LO antenna design.

IV. Methodology

Chapter II looked at reported bandwidth and computational modeling of high impedance ground plane antennas found in recent literature. This chapter details the approach used in developing and testing broadband HIGP antennas. Since this research brings together work from two separate theses, one based solely on computational modeling, the other based entirely on experimental measurements, trade-offs in design are made to satisfy fabrication requirements, along with experimental and computational limitations.

Section 4.1 derives the HIGP and bowtie antenna designs. Section 4.2 details the fabrication process. Computational methods are discussed in Section 4.3. Finally, Section 4.4 outlines measurement techniques.

4.1 Antenna Design

A two step process matches separate analytic designs of the HIGP and bowtie antenna. First, a HIGP is designed for a desired resonant frequency and bandwidth. The bowtie antenna is subsequently designed around the HIGP resonant frequency. Each step in the process comes with its own engineering approximations. As such, the design process gives a first order approximation–a starting point.

4.1.1 HIGP Design. Wilmhoff's proposed HIGP design is based on the Sievenpiper equations (1)– (6) described in Section 2.1. According to his calculations, Wilmhoff projects a HIGP resonant frequency of 3.0 GHz and bandwidth of 48%; however, an error in the calculation is noted and discussed later in this section.

The structure consists of periodically spaced triangular elements oriented between two substrates and connected to a ground plane using vias, see Figure 11. The top substrate is 1.5 mm thick, has a surface dimension of $7.63cm \times 22.9cm$, and has a relative permittivity of 2.0 within the operating band. The bottom substrate is 7.63 mm thick, has the same surface dimensions as the top substrate, and has a relative permittivity of 4.9.

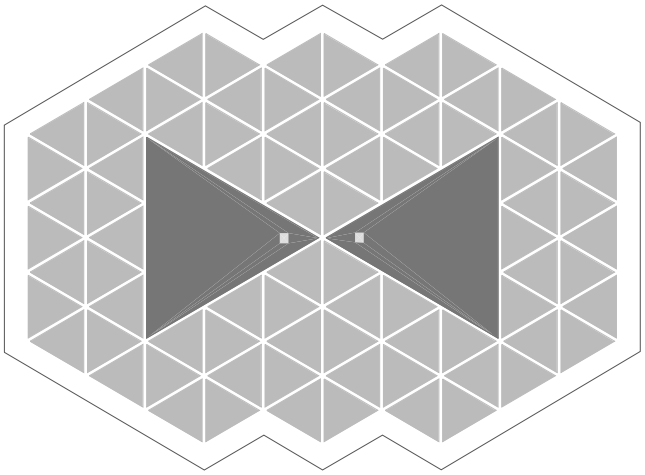

Figure 11 Top View of Wilmhoff HIGP design.

The elements are equilateral triangles with edge lengths of 8.4 mm. Adjacent elements are separated by a 0.5 mm gap, and have via-to-via spacings of 5.4 mm. The HIGP structure is mounted in a metallic cavity, with the antenna layer (described in section 2.2) flush with the top surface of the cavity. Parameters that apply to the Sievenpiper design equations are summarized in Table 5.

Table 5 Wilmhoff HIGP Design Parameters.

Parameter	Symbol	Value
Substrate thickness	t	7.63 mm
Relative Permittivity	ε_r	4.5
Element Edge Length	w	8.4 mm
Element Spacing	g	0.5 mm
Via Spacing	a	5.4 mm
Correction Factor	F	$\sqrt{3}$

An error in the proposed HIGP design is noted at this point. Using the values in Table 5 and Equations (5) and (6) in Section 2.1, the HIGP has a designed resonant frequency of 1.8 GHz and bandwidth of 28% rather than the proposed values of 3.0 GHz and 48% respectively. Whether intentional or not, Wilmhoff does not use the proper correction factor (*F*) in calculating sheet capacitance. His calculated values are obtained using a correction factor of $1/\sqrt{3}$ rather than $\sqrt{3}$; however, the former applies to hexagonal elements, while the later is the correct value for triangular elements [14]. Unfortunately, the error was not found until the final stages of this research. Much of the results in Chapter V are based on the mismatch between the antenna and HIGP.

4.1.2 Bowtie Antenna Design. A bowtie antenna is an ideal choice for a HIGP backed antenna. Its broadband characteristics are well known and it can conveniently overlay triangular HIGP elements. The second point becomes an essential feature when designing a one layer, or integrated, HIGP antenna described later.

In order to precisely overlay equilateral HIGP elements, the two halves of the bowtie must also consist of equilateral triangles. In other words, a bowtie with a flare angle (α) of 60° is required. Using experimentally determined results from Brown and Woodward [2], the maximum impedance value of a bowtie with a 60° flare angle occurs when it has an electrical length of 120°, see Figure 12. The antenna is at its first resonant wavelength at this point and reaches an input impedance of 185 + j0 Ω.

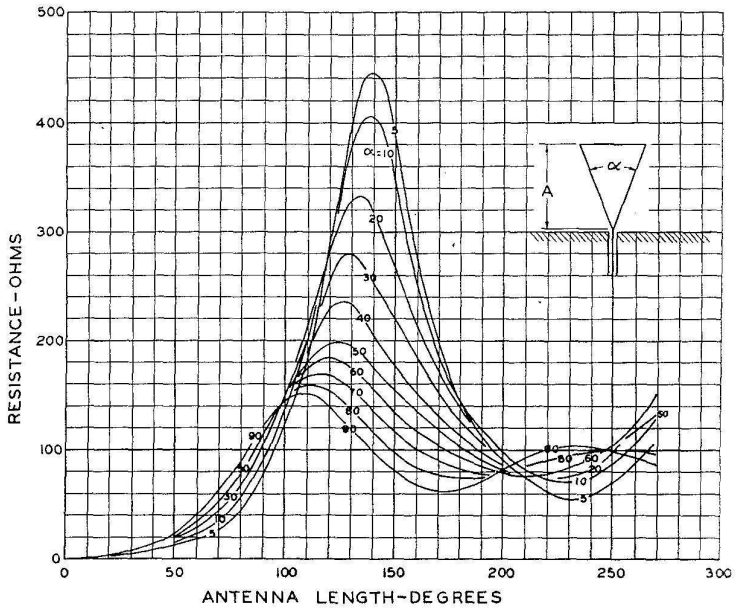

(a) Measured Resistance.

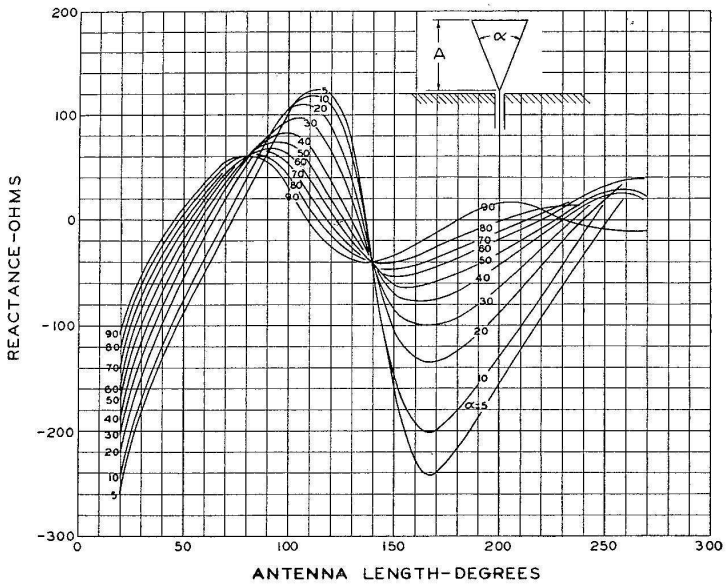

(b) Measured Reactance.

Figure 12 Measured Impedance vs. Electrical Length of Bowtie Antenna [2].

The electrical length is the product of wavelength and physical length, divided by the guided wavelength given by

$$E^{\circ} = \frac{360^{\circ}A}{\lambda_g} \tag{15}$$

where E is the electrical length in degrees, A represents the physical length in meters, and λ_g represents the guided wavelength. Separating the guided wavelength into its free space wavelength and material proprties, the bowtie electrical length is given by

$$E^{\circ} = \frac{360^{\circ}A}{\frac{\lambda_o}{\sqrt{\varepsilon_r}}} = \frac{360^{\circ}A\,f\sqrt{\varepsilon_r}}{c} \tag{16}$$

where ε_r is the relative permittivity of the antenna substrate, and λ_o, f, and c represent the free space wavelength, frequency, and velocity of light respectively.

With the resonant frequency and substrate permittivity already established in the HIGP design step, the antenna length remains as the only parameter available to optimize the bowtie antenna. Setting $E^{\circ} = 120^{\circ}$ in Equation (16), the antenna length required for a desired resonant frequency is given by

$$A = \frac{10^8}{f_o\sqrt{\varepsilon_r}} \tag{17}$$

where again A is in meters, and f_o is the free space resonant frequency.

Wilmhoff's proposed bowtie antenna has a physical length of 2.3 cm and electrical length of 118° at 3.0 GHz. The antenna precisely overlays a set of 18 triangular HIGP elements. In addition, the two halves of the antenna are feed 180° out of phase through the two centermost vias of the HIGP structure.

Bandwidth of the bowtie antenna requires no further design consideration. Brown and Woodward show that a bowtie with a 60° flare angle has a bandwidth on the order of 2:1 [2] when operating about its resonant frequency. This far exceeds the HIGP bandwidth.

The end result of the design process is a two layer structure designed to operate at a desired center frequency and bandwidth while maintaining the properties of a HIGP:

provide 0° phase shift in the reflected wave; suppress surface travelling waves. An important consideration that may be overlooked in design process is the material properties of readily available materials.

4.2 Fabrication

The fabrication process involves several "best approach" determinations. Choosing a substrate material requires more than just obtaining one of required thickness and dielectric constant. Fabrication of the HIGP and antenna layers can be accomplished by chemical or mechanical etching. Both have their advantages and disadvantages. In addition, integrating the two layers requires analyzing fabrication versus design trade-offs.

4.2.1 Material Selection. Several factors should be taken into account when selecting a substrate material. Obtaining a material of arbitrary thickness and dielectric constant can be difficult if not impossible. Readily available high frequency laminates come in standard sizes and in a limited number of dielectric constants. Materials can be custom made, but this requires bulk orders. Obtaining custom designed materials proved beyond the financial means and time constraints of this project.

A study of materials science reveals that all dielectric materials, even of the same dielectric constant and thickness, are not equal. Depending on their composition, the permittivity of any two substrates can vary quite differently with a change in temperature and frequency. As an example, the dielectric constant of FR4 varies by approximately 6% over the 1 to 5 GHz band, while the dielectric constant of Rogers RO4003 varies less than 1% over the same band [5]. Other properties that vary among materials include: dielectric breakdown, dispersion factor, loss tangent, and polarization just to name a few [8]. Loss tangent, in fact, is another important design consideration that is frequency dependent.

Materials obtained for prototypes in this research are carefully selected from product brochures of several companies. Most of the substrate materials were obtained free of charge from Rogers Corporation. Their product line includes materials with parameters

that closely match those derived in the design process. In addition, Rogers provided a wealth of knowledge on aspects of material selection and fabrication.

The two layer antenna prototypes require two different substrate materials. The bottom substrate is 300 mil thick version of Rogers TMM-4. The material is a ceramic based material and maintains a dielectric constant of 4.5 across the operating 2 GHz to 5 GHz band. The top substrate is a 60 mil thick version of Rogers RT/Duroid 5880. RT/Duroid is composed of a Teflon® based substrate and exhibits a dielectric constant of 2.2 within the desired operating band. Both materials are available in the required thickness, but neither provides the exact relative permittivities called for in design process–refer to Section 4.1 of this chapter. Material with dielectric constant of 4.9 is readily available, but not in 300 mil thickness.

Two options exist for obtaining the correct thickness and dielectric constant for the HIGP substrate: first, use a single 300 mil thick substrate (TMM-4) that has a relative permittivity of 4.5; second, stack five 59 mil thick substrates (FR4) each having a relative permittivity of 4.9. Both types of material were available. Both presented their own advantages and disadvantages. The fiberglass based FR4 has the exact dielectric constant called for in the HIGP design, but falls slightly short in the thickness parameter. The TMM-4 has the exact thickness called for in the design, but its dielectric constant is not optimum for the design. A sensitivity analysis shows the difference in performance between the two options is negligible, see Figure 13. Rogers TMM-4 is selected to avoid possible errors introduced from inconsistent gaps, warping between layers, and to ease the fabrication process.

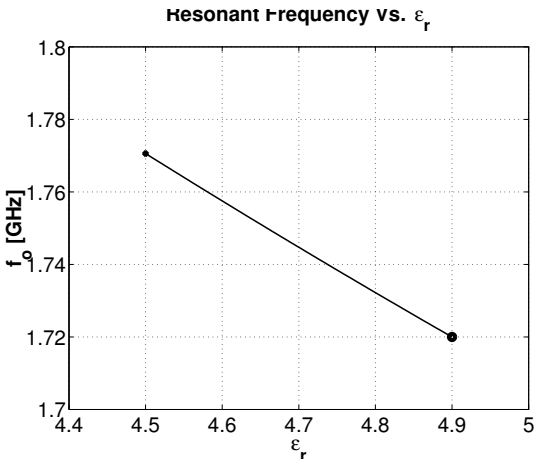

(a) Variation of resonant frequency with dielectric constant. Substrate is 300 mils thick.

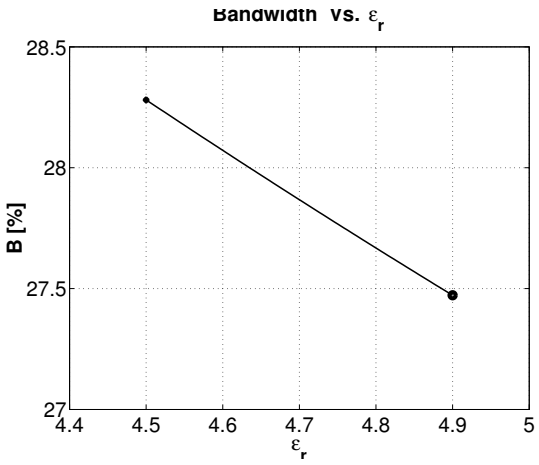

(b) Variation of bandwidth with dielectric constant. Substrate is 300 mils thick.

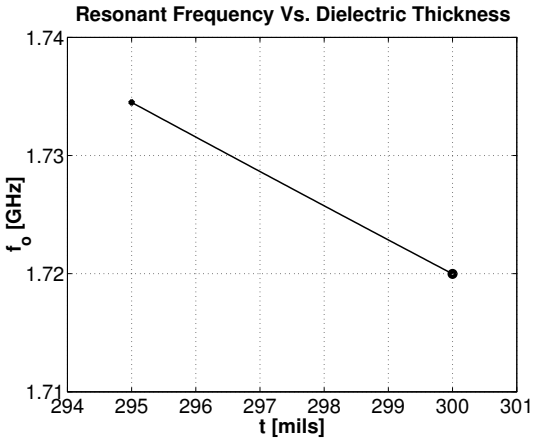

(c) Variation of resonant frequency with dielectric thickness. Dielectric constant is 4.9.

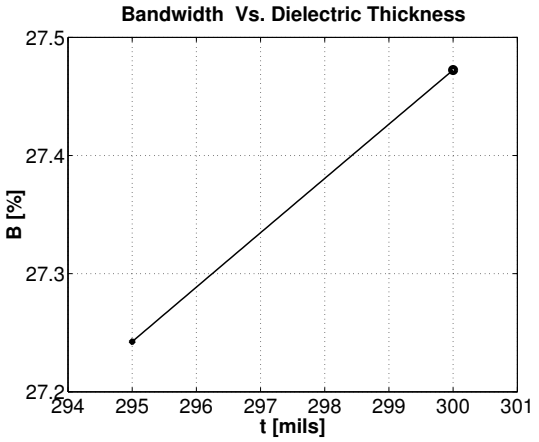

(d) Variation of bandwidth with dielectric thickness. Dielectric constant is 4.9.

Figure 13 Effect on bandwidth and resonant frequency from varying dielectric constant and substrate thickness of a HIGP.

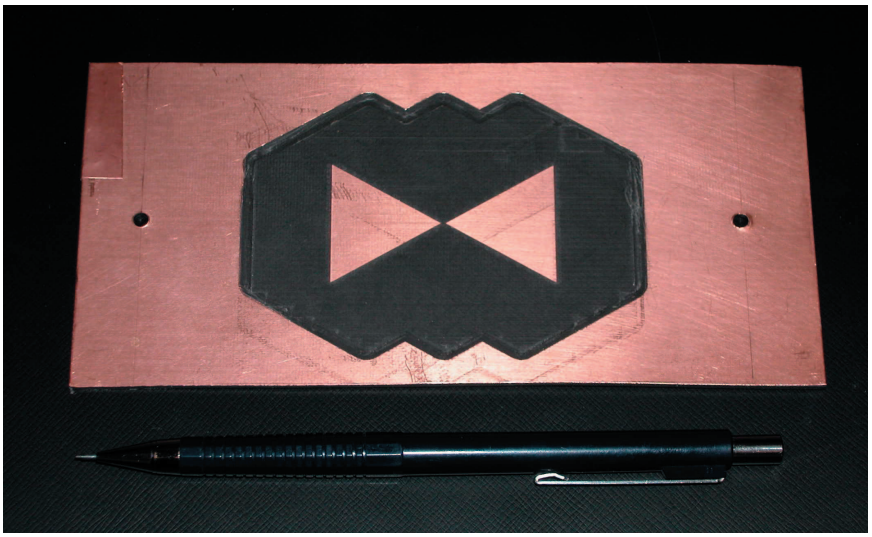

Figure 14 Top view of bowtie antenna prototype.

4.2.2 Bowtie Antenna Fabrication. The bowtie antenna is fabricated on a double clad RT/Duroid 5880 substrate, see Figure 14. The substrate is 60 mils thick and has 1-ounce copper cladding on each side. The triangular structure of the antennas is mechanically etched on one side of the printed circuit board, while the entire cladding is removed from the other side. Two holes, 40 mil in diameter, are drilled in the bowtie to accept the antenna feeds. Although all prototypes tested during this research were fabricated by means of mechanical etching, it is not the best choice for making the bowtie structure.

Mechanical etching is not ideal for removing large areas of cladding. First, it's very time consuming. Second, the process is very sensitive to equipment set-up. The circuit board must lie perfectly flat on the surface of the milling table, otherwise uneven clad and substrate removal occurs. Setting the depth of the milling router bit also plays a major role in the quality of final product. Too much depth creates rows of thin troughs in the surface, while too little depth may not fully etch cladding and inadvertently allow electrical continuity between surface elements. Chemical etching does not share the same set of drawbacks.

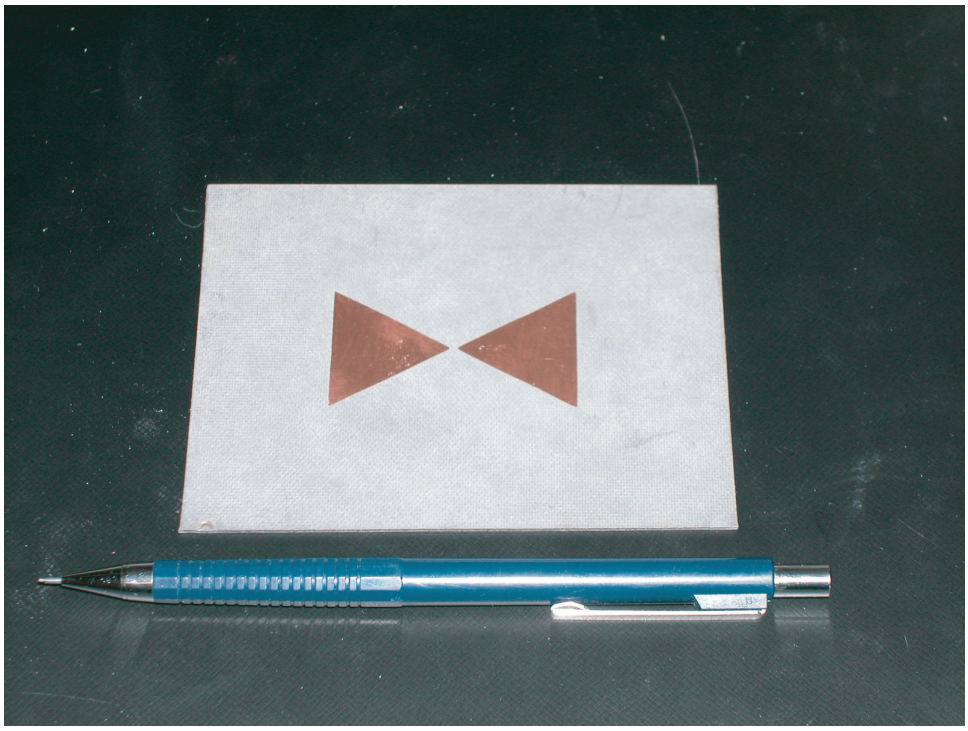

Figure 15 Chemical Etching Sample.

Bowtie patch antennas are relatively easy to fabricate using chemical etching. Several high quality antennas were fabricated by this process. As seen in Figure 15, the surfaces do not have grooves or troughs. Unlike the mechanical etching process, chemical etching only removes copper from the printed circuit board. The process results in a very smooth surface. After investing three weeks learning the equipment and process, a usable bowtie antenna could be fabricated in about 30 minutes. In the end, however, mechanical etching provided more advantages than chemical etching.

Chemical etching was abandoned for three reasons. First, the on-hand equipment could not process a 300 mil thick material–the thickness of the HIGP substrate. In addition, narrow gaps in the HIGP are much easier to etch through mechanical milling. Finally, mechanical etching allowed for more precise alignment in overlaying the bowtie onto the HIGP, as well as aligning drill holes in the two structures.

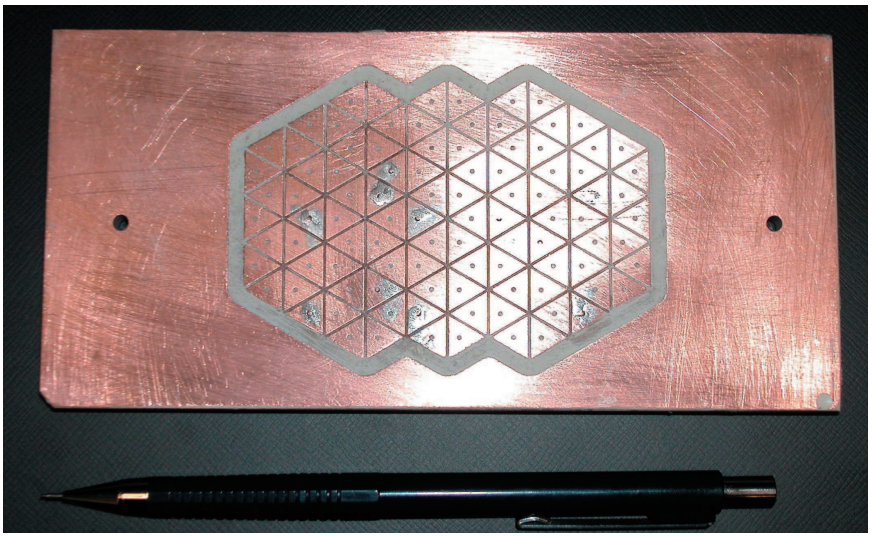

Figure 16 Top View of HIGP Prototype.

4.2.3 HIGP Fabrication. Shown in Figure 16, the HIGP is fabricated on a double clad TMM-4 substrate. The substrate is 300 mils (7.62 mm) thick and has 1-ounce copper cladding on each side. The triangular elements are mechanically etched onto one surface using a milling machine. Vias are fabricated by drilling registered holes using milling equipment, manually inserting wire into each hole, soldering the ends to each side of the substrate, and finally sanding the excess solder from the surfaces. Each HIGP required about one day to fabricate–the vias demanded the most time and labor. Unfortunately the material is too thick and dense to fabricate vias with available through-hole equipment. In addition, substituting a conductive epoxy in place of hard wires failed to produce good quality vias.

Several attempts were made at filling the via holes with a silver-filled epoxy. The epoxy, made by Epoxies Etc. (#40-3905), has a volume electrical resistivity of less than 1×10^{-4} ohm-cm. Forming vias with the epoxy is far less labor intensive, but consumes more time. The cure time of the epoxy is about 18 hours. However, the end product was less reliable than with the wire and solder method. Resistance testing of epoxy filled vias varied widely. Typical values ranged from 3 to several thousand ohms. In addition,

each fabricated board typically had a 15% failure rate (no electrical continuity) in vias. Resistance values for hard wire vias were on the order of tenths of an ohm–within the error margins of the ohm meter.

The milling equipment is software driven and requires input via a computer automated design (CAD) file. Ben Wilmhoff provided a CAD file of his proposed HIGP antenna design along with a freeware CAD package (CADStd Lite©). Minor adjustments are required after importing the design into the milling equipment's CAD software (IsoPro©). Along with CADStd© and IsoPro©, AutoCAD© is used in the the fabrication process.

4.2.4 Integrating the Structure. Final steps in the fabrication process include bonding the two substrates and attaching a feed structure. After a long conversation with Mr. Ed Sandor, Technical Representative for Rogers Corporation [13], a non-permanent bonding method was chosen over permanent bonding. The selected method simplifies fabrication. Permanent bonding methods for Teflon® based materials, such as RT/Duroid, require processes involving either specialized high temperature equipment, and/or special adhesives. On the other hand, non-permanent bonding does not require any equipment or adhesives.

Bonding is simply accomplished by applying a thin film of Vaseline petroleum jelly between the surfaces and clamping the two boards together. The Vaseline eliminates air pockets between the two boards. In addition, its dielectric constant is nearly equal to that of RT/Duroid 5880. This bonding method also allows for easy interchange of different HIGP and antenna boards.

The feed structure consists of rigid coaxial lines and a phase splitter, see Figure 17. The outer shields of equal length coaxial lines are inserted through the bottom of the HIGP board and soldered to the two inner HIGP elements. The center conductors are then soldered to the bowtie antenna. Coaxial insulation extends above the HIGP layer and slightly into the bowtie layer. This approach prevents the center conductors from shorting against HIGP elements. Finally, the coaxial lines are attached to a broadband phase shifter.

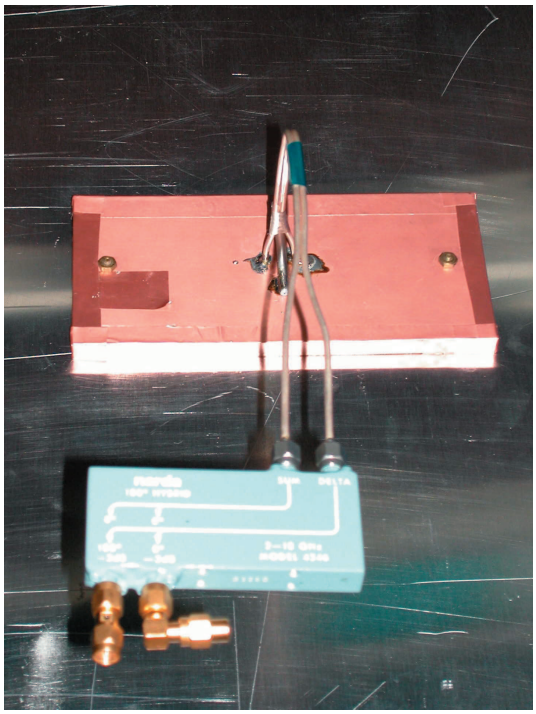

Figure 17 Antenna Feed Structure.

A Narda Broadband 180 Degree Hybrid provides the required phase shift between antenna feeds. This device splits an input signal equally and provides two outputs that have a 180° phase difference. The advertised operational band is from 2 to 18 GHz. Testing the on-hand device at 3 GHz produces the correct outputs.

The final product is then mounted in an anechoic chamber for pattern measurements. But, well before that takes place, the antenna is tested by computational methods.

4.3 Computational Predictions

The complexity of HIGP surface geometries prevents an easy closed form solution to their radiation integrals; computational predictions are instrumental in evaluating these designs.

The structures are modeled using WIPL-D and Prism. A demo version of WIPL-D enables a "quick look" at the bowtie structure over an ideal PMC ground plane. It employs

and solves the appropriate frequency-domain surface integral equation (SIE) using the moment method and entire-domain polynomial basis functions [7]. It has the advantage of fast run times. Using a single processor, 1.3 GHz, 640 MB RAM personal computer, a typical run time is on the order of minutes for a solution of 700 unknown currents. On the other hand, the demo version cannot solve the number of unknowns involved in the HIGP structure.

Prism is a FORTRAN based code that provides greater flexibility and capability. It is a finite element-boundary integral (FE-BI) program designed for conformal, slot and cavity, antenna analysis [17]. A disadvantage is that individual run times are on the order days for the models simulated in this thesis. This, despite the fact that Prism frequency sweeps were divided into 16 sub-bands of 4 frequencies each and run on multi-processor high performance computers. In addition, the process of analyzing an antenna in Prism requires several steps using additional software, see Figure 18.

4.3.1 Antenna Radiation Pattern. Frequency sweep and pattern-cut measurements are conducted using WIPL-D and Prism. Frequency sweeps are performed across the 2 to 5 GHz band. The frequency steps range between 10 to 250 MHz depending on the particular circumstances. For instance a 10 MHz frequency step is used where there is a high rate of change in gain verse frequency. On the other hand, a 250 MHz step is sufficient in many parts of the frequency band.

Pattern-cut data is computed during the same run as the frequency sweeps. The calculations cover the the top hemisphere of the antenna. For Prism, this covers the elevation (θ) range of -90° to 90°. In the WIPL-D coordinate system, the top hemisphere is covered by the elevation range of 0° to 180°. Both programs use the positive x-axis at z = 0 as the $\phi = 0^\circ$ coordinate. All computational runs collect both H-plane and E-plane data.

4.3.2 Input Impedance and Return Loss. The computational results are based on a 50 Ω characteristic line impedance, but a matched line and antenna impedance condition is simulated through post processing. First, a band containing the broadest resonance

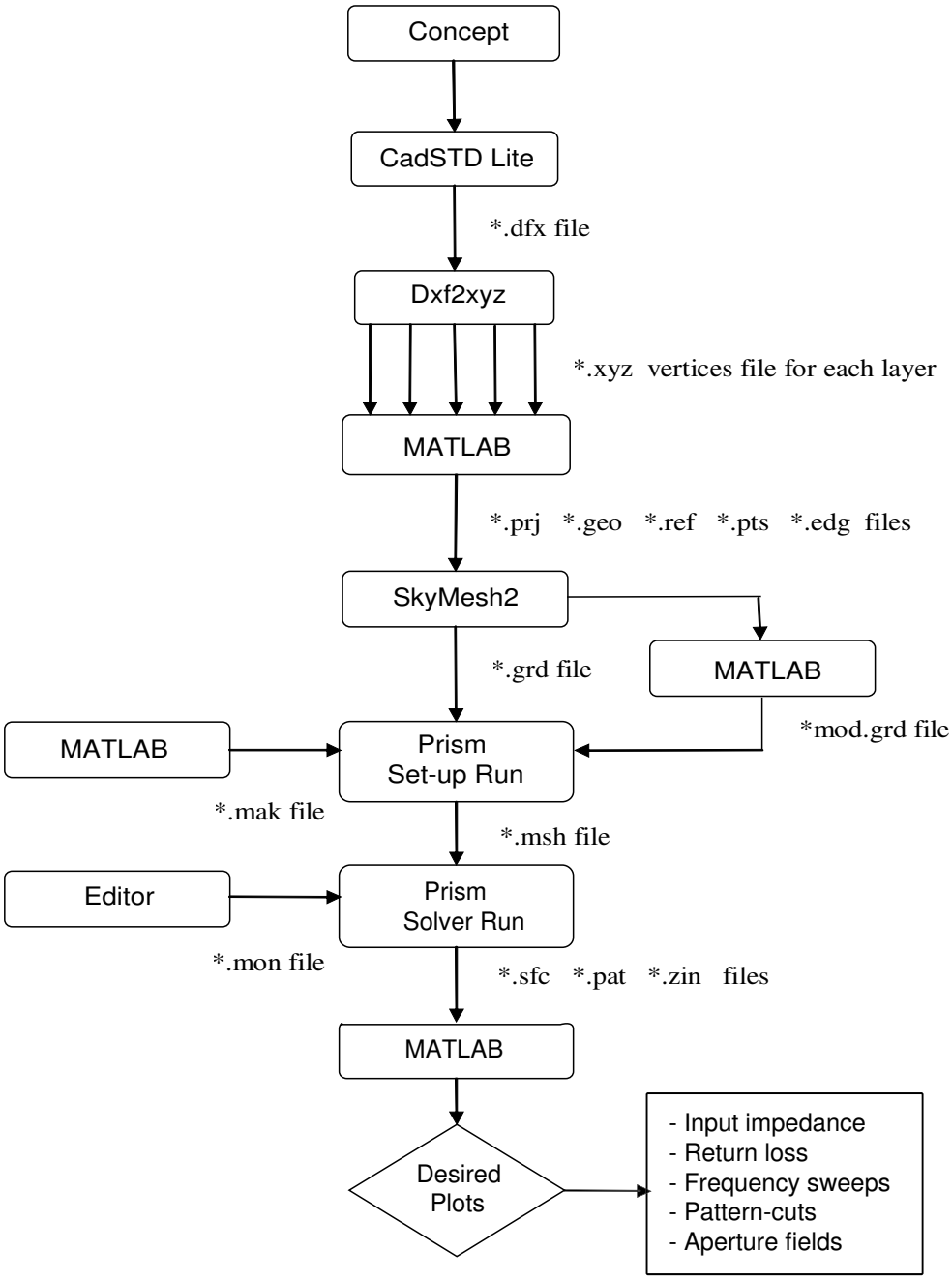

Figure 18 Prism Modeling process. Required I/O files of each stage are identified with (*.). MATLAB function required for I/O interface between programs and data processing for plotting.

region is selected from computed input impedance. Referring to Figure 19, a good choice is the band from 3.5 to 4 GHz. It is close to the desired operating frequency and has broadband characteristics; the peak of Re$\{Z_{\text{in}}\}$ is relatively broad, and the Im$\{Z_{\text{in}}\}$ goes through a zero cross-over at a relatively low rate of change with respect to frequency. Next, the input impedance data is converted to return loss by replacing the characteristic impedance value of 50 Ω to a value that best matches the impedance in the selected operating band. Using transmission line theory [9], input impedance is converted to return loss by

$$\text{RL} = -20\log_{10}|\Gamma| = -20\log_{10}\left|\frac{Z_L - Z_0}{Z_L + Z_0}\right| \tag{18}$$

where RL is return loss in dB, Γ is the voltage reflection coefficient, Z_L is antenna input impedance, and Z_0 is the characteristic line impedance. So, using Equation (18), the computed input impedance data is converted to return loss by replacing the characteristic impedance value of 50 Ω to a value that best matches the impedance at the peak of the resonance band.

4.3.3 Bandwidth. Antenna bandwidth is calculated as a -9.5 dB return loss band about the operating frequency. The bandwidth is expressed as a percentage is given by

$$B = \left(\frac{f_U}{f_L} - 1\right)100 \tag{19}$$

where B is bandwidth, f_U is the upper cut-off frequency, and f_L is the lower cut-off frequency.

As with the design process, computational models involve assumptions and approximations. Experimental measurements can provide strong support to antenna synthesis.

4.4 Experimental Measurements

The AFIT microwave laboratory provides all necessary equipment to evaluate the HIGP antennas. The anechoic chamber allows accurate radiation pattern measurements,

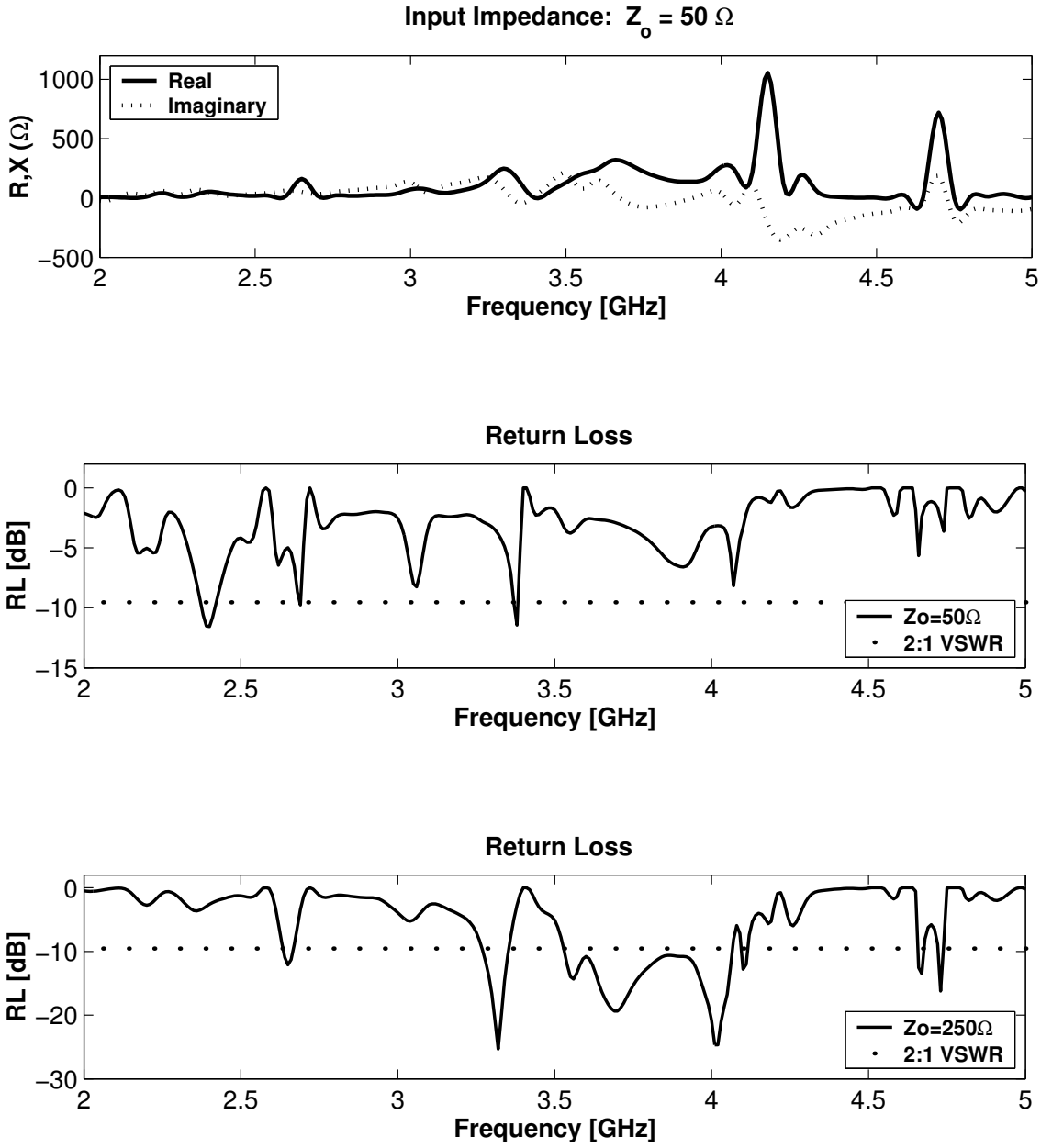

Figure 19 Example of impedance matching. Computational results of input impedance Z_{in} (top), return loss using a characteristic impedance of 50 Ω (middle), and return loss recalculated under a matched impedance condition (bottom).

while other equipment such as network analyzers allow a "quick look" at the various antenna characteristics.

The anechoic chamber utilizes an HP8510B Network Analyzer, a standard gain horn, a mechanical turntable, and a personal computer. The Network Analyzer and turntable are computer-controlled using National Instruments' Labview® software, see Figure 20. Antennas under test are mounted in a metallic circular test body. The geometry of the test body reduces edge diffraction and approximates scattering from an infinite PEC plane. The test body is supported by a foam column.

The following coordinate system applies to antenna measurements in the chamber: the antenna surface is in the XY-plane, and the rotation, or azimuth, is in the θ direction with antenna broadside at $\theta = 0^\circ$. Changing between horizontal and vertical polarizations is accomplished by rotating the horn antenna by 90°.

4.4.1 Antenna Radiation Pattern. Similar to the RCS measurements described in chapter III, antenna performance is characterized using two types of S21 measurements: frequency sweeps and pattern-cuts. Frequency sweeps are conducted over the 2 to 5 GHz band and with the antenna oriented at $\theta = 0^\circ$. The frequency band is swept at 3.75 MHz intervals providing 801 data points within the measured band. Antenna pattern-cut measurements are taken over an azimuth range of -90° to 90° at 1° intervals.

Both E-plane and H-plane measurements are conducted for all frequency sweeps and pattern-cuts. Data from each measurement is imported into MATLAB© for post-processing and plotting. In addition, data is calibrated using the calibrated response of a second standard gain horn.

Prior to conducting radiation pattern measurements, each antenna is tested on a stand alone HP8720C Network analyzer.

4.4.2 Return Loss and Input Impedance. Return loss measurements are conducted across the same band and interval as the frequency sweeps, 2 to 5 GHz and

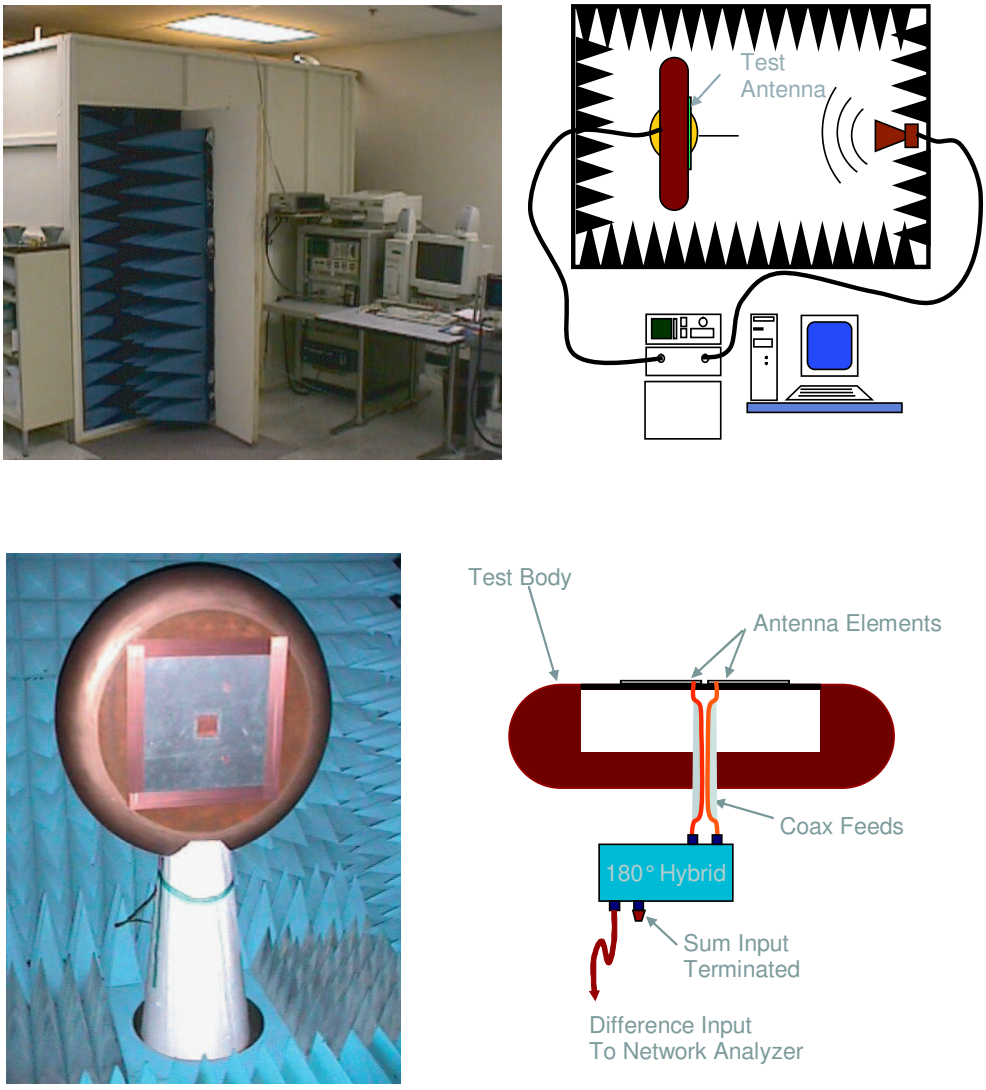

Figure 20 AFIT mini-chamber: External view of chamber (top left), Functional diagram of chamber and associated equipment (top right), Internal view of chamber (bottom left), Diagram of test body (bottom right).

3.75 MHz respectively. The S11 measurements provide return loss data, which in turn provides antenna input impedance and, to some extent, resonant frequency data. Results are presented in the form of return loss versus frequency and in the form of Smith Charts.

4.4.3 Bandwidth. The bandwidth is estimated through post processing of the return loss data. As with the anechoic chamber measurements, all network analyzer measurements are referenced to a 50 Ω characteristic line impedance. Input impedance of the HIGP antennas under test are in the 200 to 500 Ω range. The mismatch in impedance between the antennas and transmission line shows up as narrow operating bands in the return loss plots. An operating band is defined as a band of frequencies with a -9.5 dB or greater return loss. The same process of simulating a matched impedance condition used in computational data is also applied to the experimental data.

V. Results and Analysis

Chapter IV presented computational and experimental methods used in evaluating antennas. This chapter presents results using such methods. Several types of antennas are measured and evaluated. In some cases analysis is based on results from both computational and experimental methods presented in Chapter IV. In other cases only experimental results or computational results were obtained.

An iterative design approach is used in developing the antennas. First the antenna is modeled and tested through computational methods. Next, a prototype is fabricated having the same dimensions and material parameters as derived in the analytic design stage. Next, modifications to the antenna occur based on analysis of measured results. In addition, individual layers of the structure of known characteristics, such as the bowtie over a substrate, are measured separately to evaluate the accuracy of the modeling process. In an ideal case, the entire process is repeated with the development and testing of a refined prototype. Time did not allow refinement of antennas in most cases.

5.1 Bowtie above Substrate and PEC Ground Plane

Computational and experimental measurements of a simple bowtie antenna over a substrate and PEC ground plane provides an answer to a key question: How well do results match between the two computational methods and experimental methods? Although time did not permit fabrication and experimental measurement the antenna, results and analysis of the two computational methods are provided in the following sections.

5.1.1 WIPL-D Results. WIPL-D allows a quick and easy analysis of the antenna, but it is also the least robust of the methods. Since the demo version is limited to a maximum of 700 unknown currents, a "basic model" is used in modeling the structure as shown in Figure 21. A limit in the electrical size also required the substrate to be reduced to physical dimensions of 3.3"$\times$2.35" rather then the fabricated and Prism model dimen-

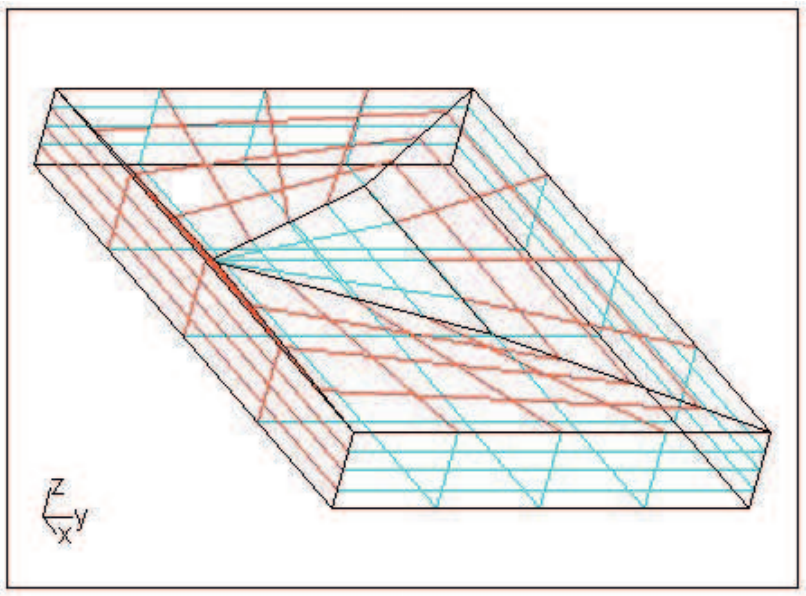

Figure 21 WIPL-D model of bowtie antenna over substrate and ground plane. Green mesh represents metallic plates, red mesh represents substrate material. As shown, symmetry allows modeling 1/2 of structure.

sions of 6"×3". The bowtie is $120°$ at 3 GHz and has a flare angle of $60°$. Symmetry about the X-axis allows modeling of only one half of the structure. The bowtie, feeds, and finite ground plane consists of infinitely thin composite metallic plates. Dielectric plates form the outer boundaries of the substrate. The substrate is modeled with a dielectric constant of 4.5 and thickness of 300 mils. Current is provided via the basic generator option set to an amplitude of one volt. The voltage is fed at the center of the wire connecting the two halves of the bowtie. The result is a $180°$ phase difference in current between the two halves.

The computational results are in very good agreement with the analytical design. The antenna has a resonant frequency of 3.0 GHz which matches the value derived in Section 4.1.2, see Figure 22(a). The imaginary part of input impedance has a zero crossover at 3.0 GHz, while the real part has a peak resistance of 265 Ω at 2.85 GHz. Referring to Figure 22(b), matching the antenna to a 250Ω line impedance results in a -9.5 dB return loss band from 2.3 to 3.15 GHz. The 37% bandwidth is lower than the predicted HIGP

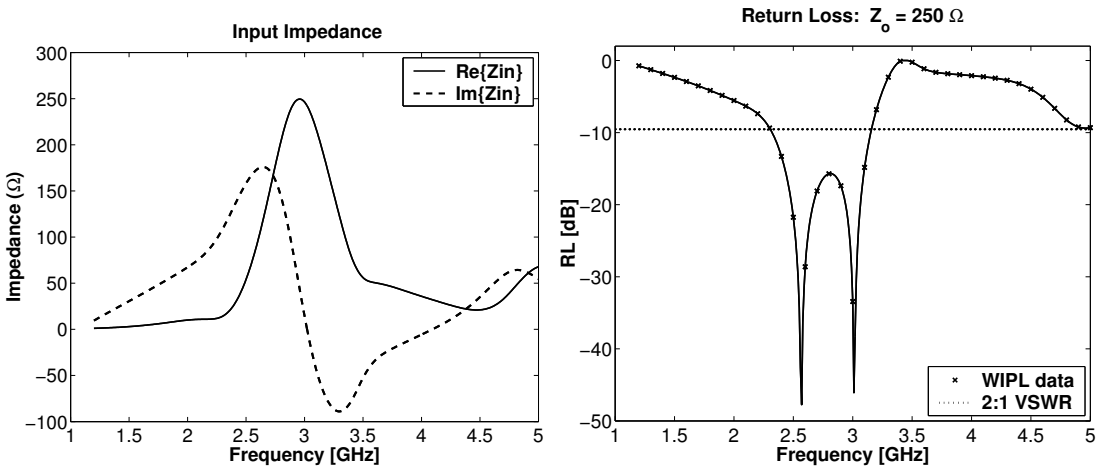

(a) Input Impedance.

(b) Return Loss.

Figure 22 WIPL-D: Input impedance and return loss of bowtie antenna over 300 mil thick, D.K. 4.5 substrate and PEC ground plane. Return loss calculated under matched impedance condition.

bandwidth (48%) of the Wilmhoff two-layer HIGP design and would therefore limit the bandwidth of the combined HIGP and bowtie antenna structure.

The 265 Ω peak resistance value is higher than the value (185 Ω) experimentally measured by Brown and Woodward for an antenna of the same electrical length ($120°$) and flare angle ($60°$), see Figure 12 in Section 4.1.2. The difference in input impedance may be attributed a difference in feed locations, and in the fact that the bowtie is mounted on top of a substrate rather than in air.

Antenna pattern-cuts at 2.3 GHz are shown in Figure 23(b) and 23(c). A peak gain of 5 dB gain occurs at broadside [WIPL-D coordinate system puts broadside at $\theta = 90°$]. The broadside gain from 1 to 5 Ghz is shown in Figure 23(a). Unlike return loss values, the gains are not recalculated under a matched impedance condition. Higher antenna gain can be expected when the bowtie input impedance is matched to the line impedance.

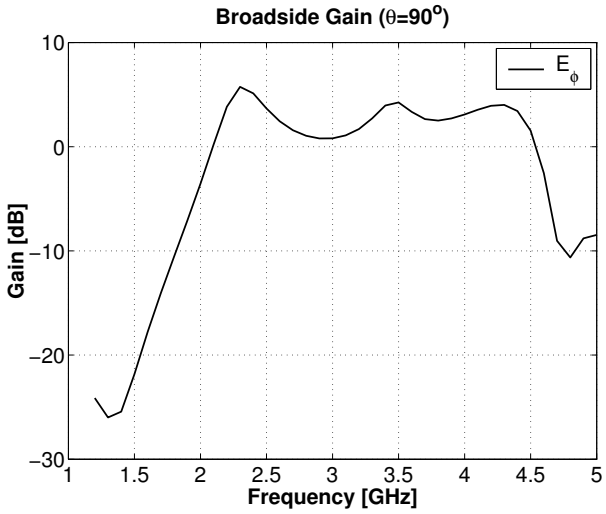

(a) Broadside gain.

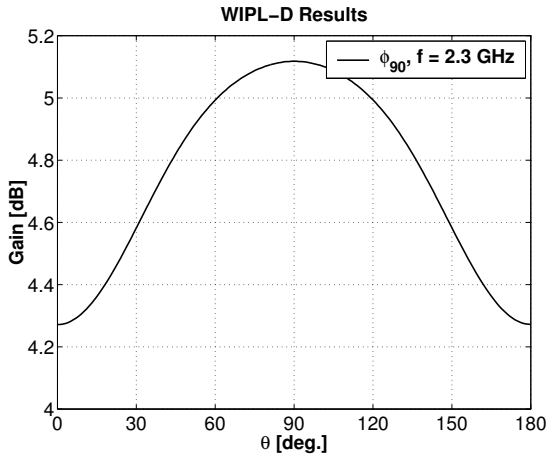

(b) H-plane Radiation Pattern.

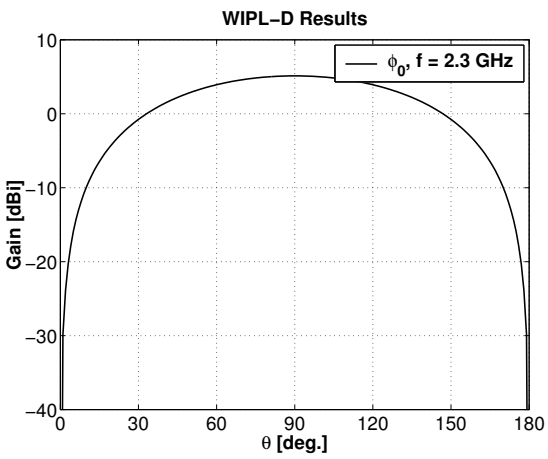

(c) E-plane Radiation Pattern.

Figure 23 WIPL-D broadside gain and 2.3 GHz radiation patterns.

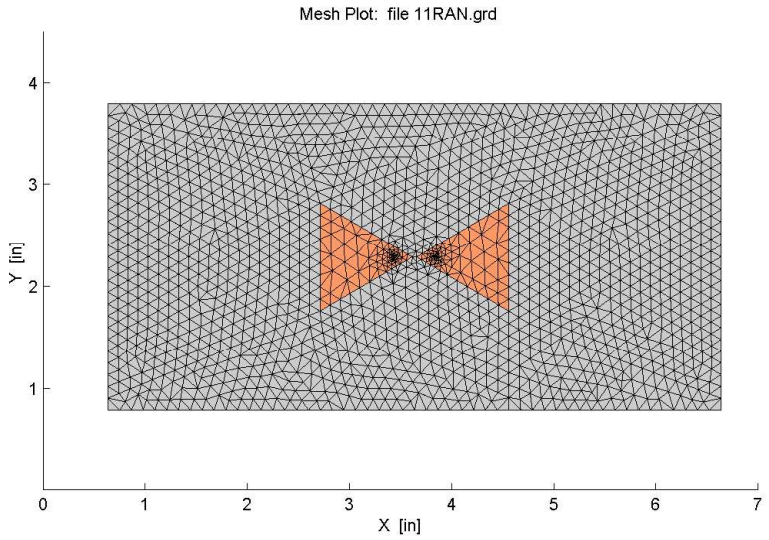

Figure 24 Prism Model, Top view of bowtie antenna over substrate and ground plane. Copper mesh represents metallic plates, gray mesh represents substrate material.

5.1.2 Prism Results. The Prism model is more representative of the actual bowtie prototype. First, the antenna is modeled as a cavity-backed surface mount antenna. It is bottom fed with feeds modeled in the same locations as the prototype. The substrate has a dielectric constant of 4.5 and dimensions of 6"$\times$3"$\times$0.3". The bowtie The bowtie is 120° at 3 GHz and has a flare angle of 60°. However, as with WIPL, metallic surfaces are modeled as PEC plates and substrates are modeled as a lossless dielectric. See Figure 24 for mesh diagram.

Comparing the WIPL and Prism models, Figures 21 and 24, the bowties are not oriented along the same axes. The bowtie is symmetric about the x-axis in the WIPL model and is symmetric about the y-axis (with a 3.6" offset) in the Prism model. As such, radiation patterns are referred to in terms of E-plane and H-plane patterns rather than in terms of ϕ_0 and ϕ_{90} pattern cuts. The E-plane and H-plane are the planes containing the electric field and magnetic field vectors respectively [16]. Referring to Figure 24, the E-plane is the XZ-plane that cuts through the centroid of each bowtie halve. The H-plane is perpendicular to the E-plane and cuts through the center of the bowtie tips.

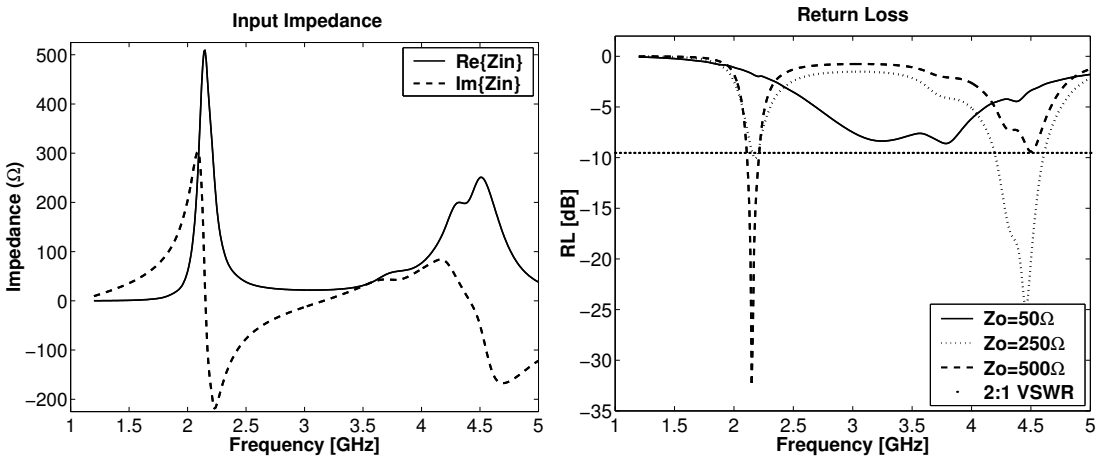

(a) Input Impedance.

(b) Return Loss.

Figure 25 Prism input impedance and return loss of bowtie antenna over 300 mil thick, D.K. 4.5 substrate and PEC ground plane.

The Prism results are in poor agreement with the designed performance and WIPL results. The antenna achieves resonances at 2.2 GHz and 4.4 GHz rather than at the intended 3.0 GHz. Referring to Figure 25(a), the antenna is poorly matched to a 50 Ω line impedance. In fact, the return loss is above -9.5 dB through-out the 1.2-5 GHz band, see Figure 25(b). In terms of standing waves, the antenna VSWR is greater than 2:1 across the entire band. The *impedance mismatch factor q* may be used to further highlight the poor efficiency of the antenna. The mismatch factor is a figure of merit identifying the fraction of power transferred at the antenna feed and transmission line junction [16]. The *q* factor is given by

$$q = 1 - |\Gamma|^2 = 1 - \left| \frac{Z_L - Z_\circ}{Z_L + Z_\circ} \right|^2 \tag{20}$$

where *q* is the impedance mismatch factor, Z_L and $Z_\circ$ are the antenna input impedance and line impedance, respectively in ohms. The simulated results achieve a *q* factor of 0.33, or 33% at the 2.2 GHz resonance. A significant portion of the transmit signal does not cross the antenna feed junction.

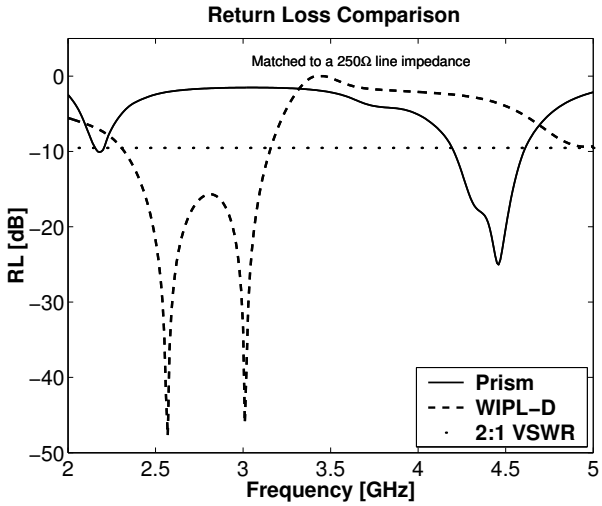

(a) Return Loss.

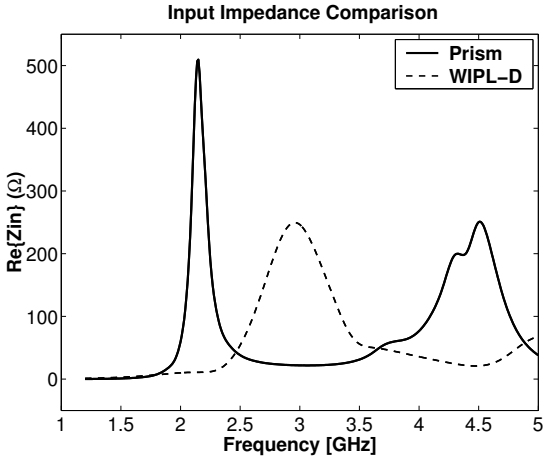

(b) Input Impedance: Resistance.

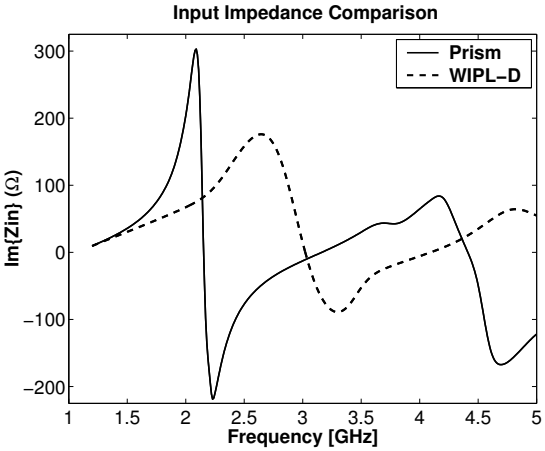

(c) Input Impedance: Reactance.

Figure 26 Return loss and input impedance comparisons: WIPL-D vs. Prism.

Although the peak input impedance (250Ω) at the second resonance is the same value as computed in WIPL, the bandwidth is much lower. Matching the antenna to a 250 Ω transmission line provides a -9.5 dB band from 4.2-4.6 GHz (9.5%), see Figure 26(a). The Prism model results in a bandwidth that is about 1/4 of that computed in WIPL.

The broadside gains of each model do not show agreement, but do reveal a common gain at 2.3 GHz 27(a). The radiation pattern results compare favorably when both methods have an overlapping operating band. As shown in Figure 27(b) and 27(c), the WIPL and Prism pattern cuts are very similar in form. The E-plane patterns nearly overlap while the H-plane patterns differ by less than 0.5 dB at broadside. In fact the H-plane patterns differ no more than 1.5 db at all elevations. The WIPL H-plane pattern has the least variance across all elevations and is very close to a constant (isotropic) gain. NOTE: The WIPL elevation coordinate system was changed to match that of Prism i.e broadside at $\theta = 0^\circ$ rather than at $\theta = 90^\circ$.

Overall, the two computational methods do not match well, but do produce similar results in limited cases. Possible causes in dissimilarities are differences in modeling geometry and fed methods. The Prism model not only has a larger surface area, but also is configured as a cavity mount antenna. The WIPL model is configured with substrate enclosed in a metallic box which rests on top of a ground plane. The two models should have different behaviors at their respective substrate boundaries. The difference in physical sizes also leads to different resonant modes within the enclosed substrate cavities. Finally, the differences in modeling the feeds can have a significant impact on the input impedance.

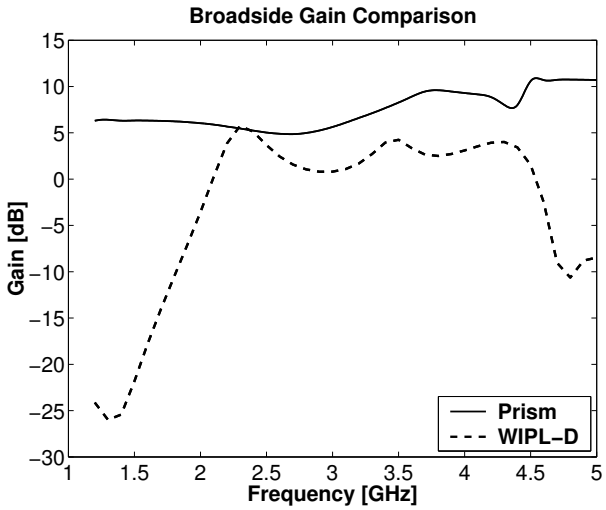

(a) Broadside Gain.

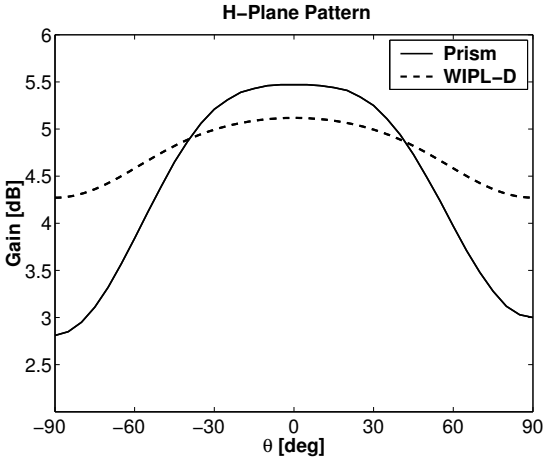

(b) H-plane Radiation Pattern.

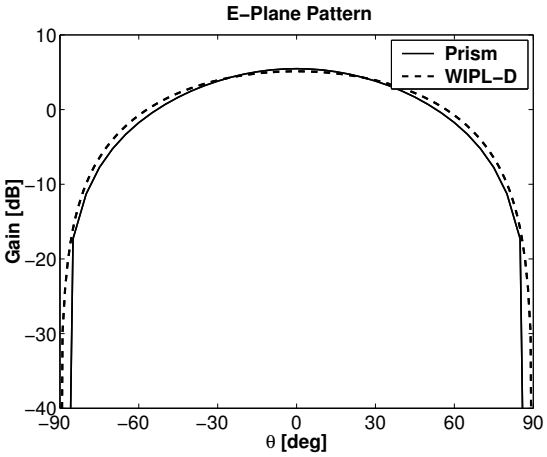

(c) E-plane Radiation Pattern.

Figure 27 Broadside gain and radiation pattern comparisons: WIPL-D vs. Prism.

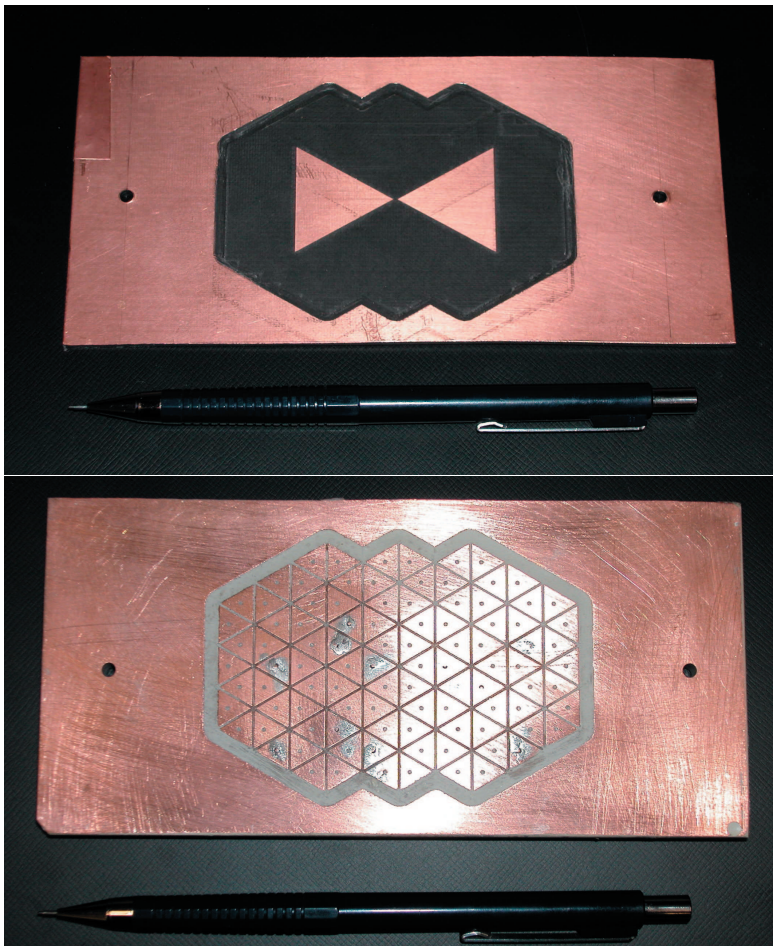

Figure 28 Bowtie antenna (top) and HIGP (bottom) layers of two-layer HIGP antenna design.

5.2 Bowtie above Substrate and HIGP

The primary goal of this thesis was to demonstrate a relatively large bandwidth HIGP antenna through both experimental and computational methods. Unfortunately the computational methods were unable to model the two-layer design, and a design error prevented any useful analysis of the measured results. The error was noticed too late in the research to allow fabrication and testing of a corrected design, but a new two-layer design is developed analytically and presented.

5.2.1 Measured Results. The bowtie antenna is designed for a 3 GHz resonant frequency and has an estimated 50% bandwidth. The HIGP design error leaves it with a 1.8 GHz resonant frequency and 28% bandwidth rather than the proposed values of 3.0 GHz and 48% respectively. The mismatch in the operational bands of the two structures effectively attenuates fields at the antenna. The structure behaves like two bandpass filters in series that are tuned for greatly separated bands. Although measured results of the Wilmhoff design are presented in Figure 29, they do not support any useful evaluation.

5.2.2 Introduction of New Two-layer Design. The design error presented an opportunity to develop a design based on lessons learned during past fabrication and modeling efforts. Besides matching the resonant frequency of the bowtie and HIGP, the new design eases the fabrication process and reduces the electrical size in thickness–beneficial in computational modeling.

The overriding philosophy during the process was to design around materials that are both readily available and easy to work with. The thick ceramic substrate presented several obstacles: could not chemically etch, automate drilling, use through hole platting, or use conductive epoxy for vias. The material also requires special tools in order to cut. The new design calls for a much thinner substrate and uses the same family of Teflon® based material as the top substrate. Since bandwidth decreases with a decrease in substrate thickness, a conscious trade-off was made between bandwidth and substrate thickness.

A secondary goal was to preserve the current surface geometry. Minimizing changes in the geometry requires only minor modifications to the computational model and allows the bowtie to remain over the same number of HIGP triangular elements. The only changes in geometry involve the gap spacing, and subsequently the via spacing. The gap was changed in-order to fine tune the resonant frequency and allow use of a standard size milling bit. In addition, the change in gap spacing results in a slight, but negligible, change in the bowtie length. See Table 6 for a comparison of the original and new design specifications.

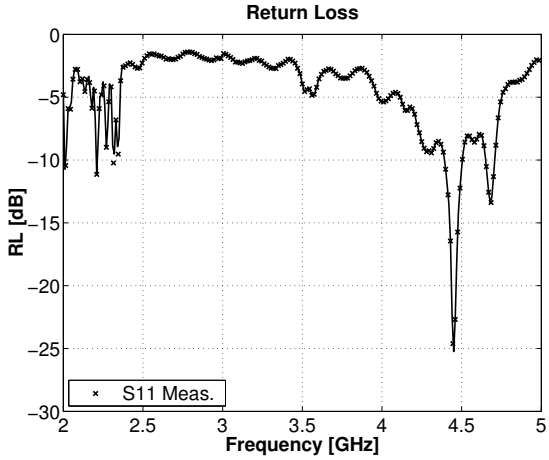

(a) Return Loss.

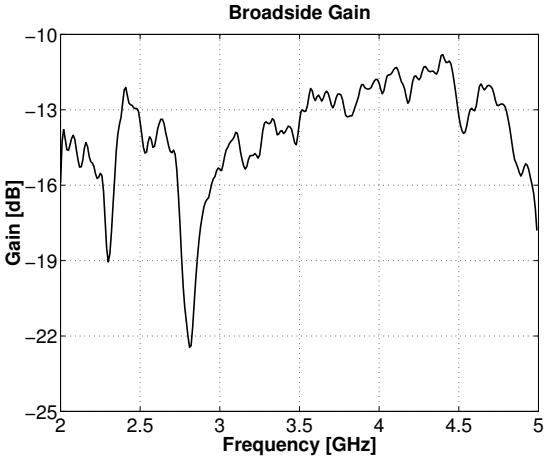

(b) Broadside Gain.

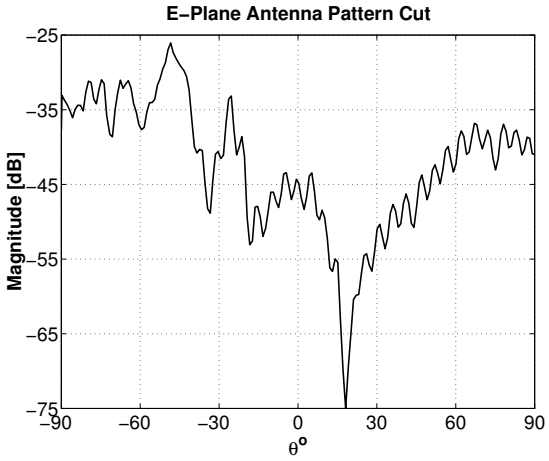

(c) Radiation Pattern.

Figure 29 Measured return loss, broadside gain, and 4.475 GHz radiation pattern of two-layer design. HIGP and bowtie resonant frequencies mismatched.

Table 6 Original and New HIGP Design Parameters.

Parameter	Symbol	Original Design	New Design
HIGP resonance	$f_\circ^H$	1.77 GHz	3.03 GHz
Bowtie resonance[1]	$f_\circ^B$	3.0 GHz at 118°	3.0 GHz at 121°
HIGP bandwidth	B	28%	20%
Substrate thickness	t	300 mils	125 mils
Relative Permittivity	ε_r	4.9[2]	2.35
Element Spacing	g	19.7 mils	10 mils
Via Spacing	a	212 mils	202 mils
Bowtie length	A	2.30 cm	2.25 cm

Although the new two-layer HIGP antenna design was neither tested, nor analyzed, the one-layer version of the antenna was modeled. The results are quit promising.

5.3 Bowtie Integrated into HIGP Surface

In this section, a one-layer, or integrated, version of Wilmhoff's two-layer HIGP bowtie antenna is investigated. The antenna is placed in the plane of the HIGP rather than above it. Golla introduced the concept in his thesis research of HIGP backed log-periodic antennas in 2001 [4]. Two designs are analyzed: one using the original two-layer design parameters, and one using the new parameters.

The integrated structures are very similar in design to the two-layer structures. The HIGPs use the same design parameters as in the two-layer versions, see Tables 5 in Section 4.1.1 and 6. The bowtie replaces 18 triangular elements in the HIGP layer. The second substrate layer that contains the bowtie in the two-layer design is completely removed.

5.3.1 Original One-Layer Design. Computational results alone show that the integrated antenna does not achieve the predicted 28% bandwidth. Using the 9.5 dB return loss bandwidth as the figure of merit, the antenna operates efficiently from 3.53 to

[1]First resonance of a bowtie with a 60° flare angle occurs when electrical length is 120°

[2]Material with permittivity of 4.5 was used during evaluation of original design. Material with permittivity of 4.9 and thickness of 300 mils was not readily available.

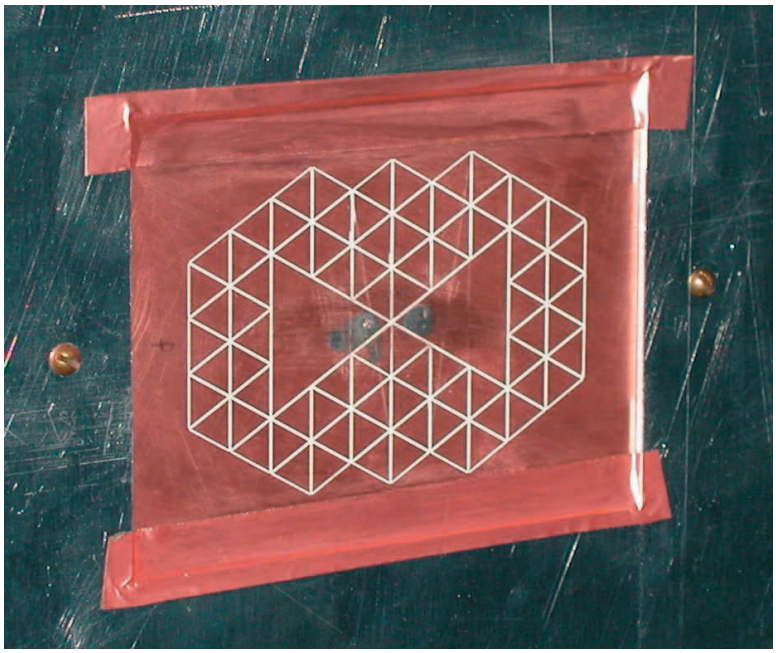

Figure 30 One-layer HIGP antenna mounted in antenna test chamber. Early prototype: no vias and thin isolation boundary between HIGP and cavity.

4.11 GHz, see Figure 31. The calculated bandwidth, f_u/f_ℓ, where f_u and f_ℓ are the upper and lower cut-off frequencies is 16.4% centered at 3.82 GHz. Considering the mismatch in operating bands of the HIGP and bowtie, a bandwidth of 16.4% is relatively high.

The broadside gain and antenna radiation patterns at 3.75 GHz are shown in Figure 32. All results are based on a characteristic input impedance of 50 Ω. The widest operating band is clearly in the 3.5 to 4 GHz range at which a gain of about 11 dBi is achieved. Higher gain can be expected when the antenna is matched to a 250Ω line impedance.

Measured results do not duplicate computational reults for the most part, see Figure 33. Measured return loss does track Prism results in some areas of the 2-5 GHz band, but other results are less similar. Gain patterns require more effort to adequately compare results. Data from the antenna range measurements were not calibrated. As such, both computational and experimental gain data were normalized in order to allow analysis of

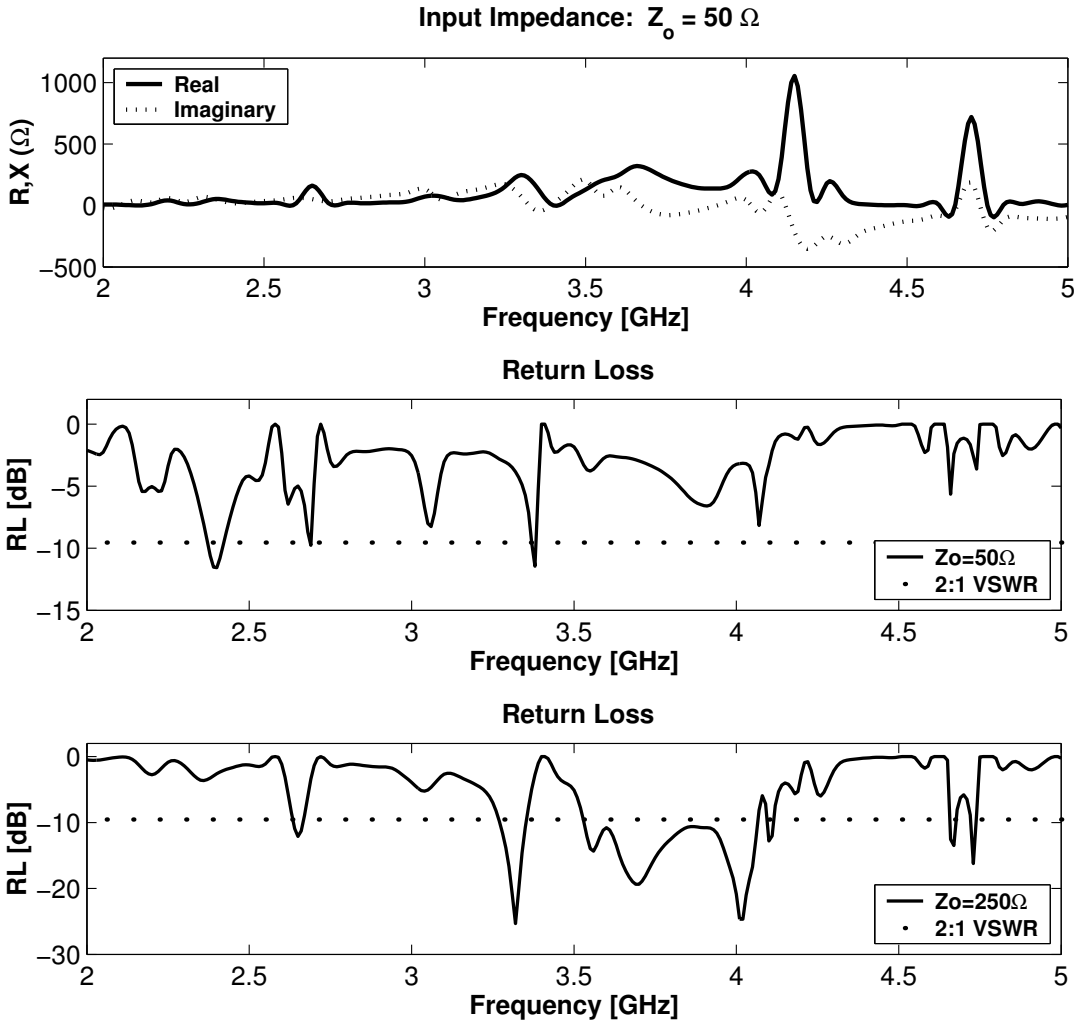

Figure 31 Prism results of input impedance (top), return loss with a line impedance of 50 Ω (middle), and return loss at matched impedance condition (bottom).

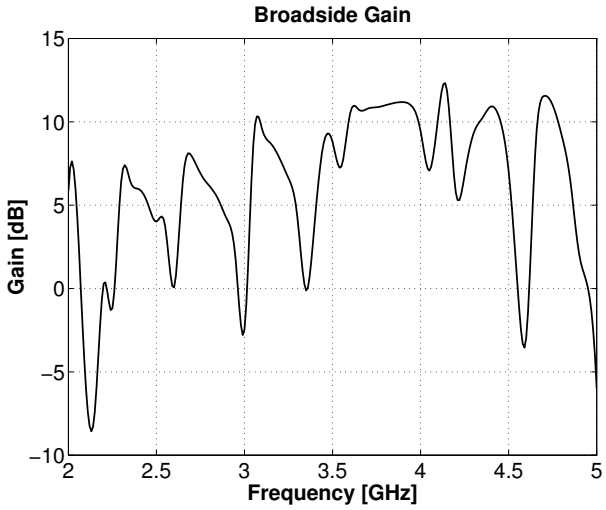

(a) Broadside Gain.

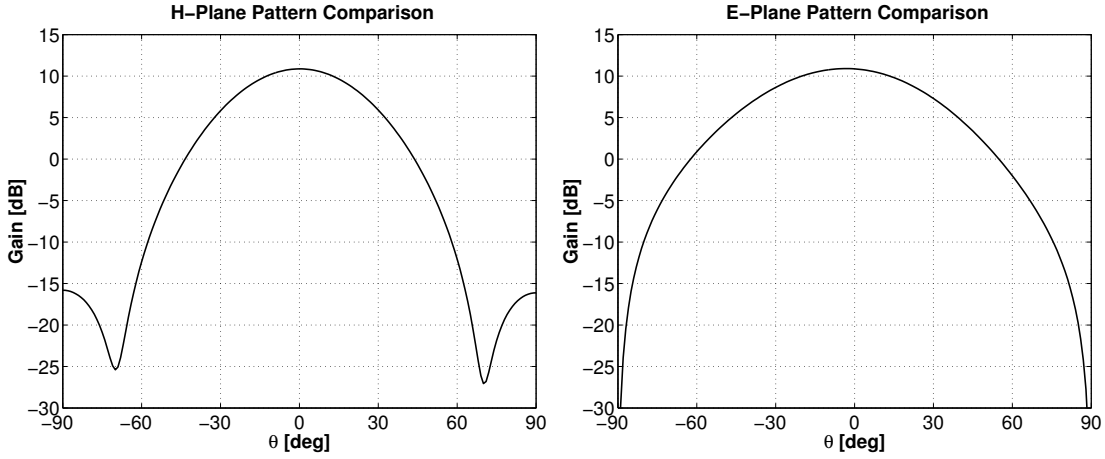

(b) H-plane Radiation Pattern.

(c) E-plane Radiation Pattern.

Figure 32 Prism broadside gain and 3.75 GHz radiation patterns of original one-layer design.

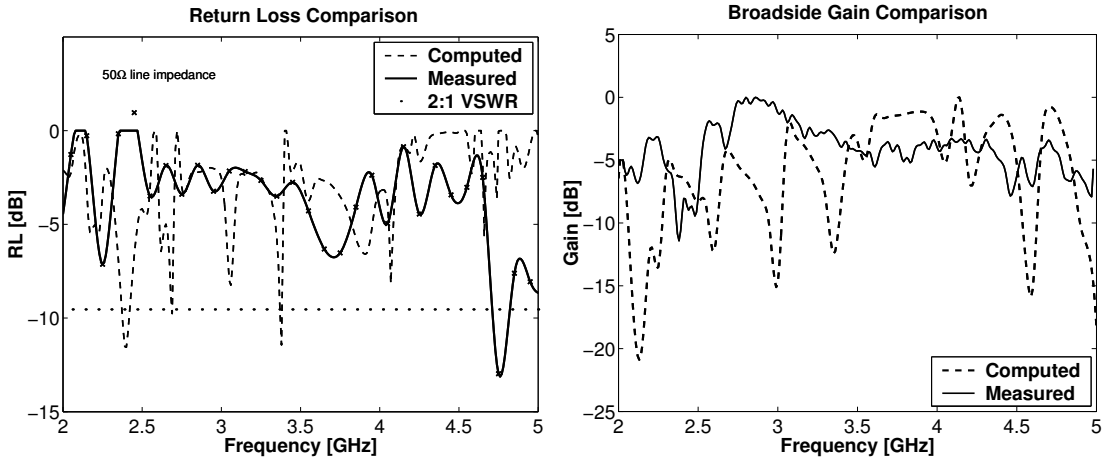

(a) Return Loss.

(b) Broadside Gain.

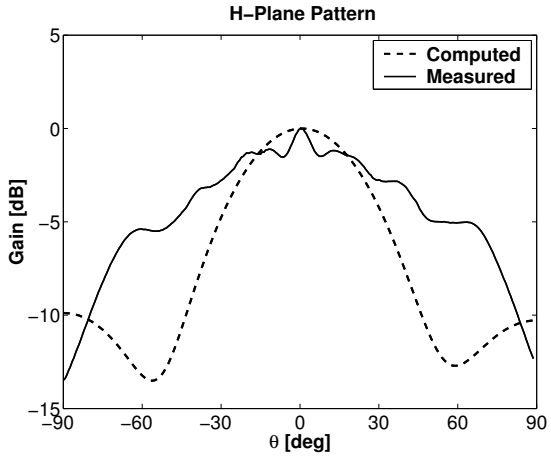

(c) Radiation Pattern.

Figure 33 Measured and computed return loss, broadside gain, and 2.65 GHz radiation pattern. Characteristic impedance of 50Ω.

the general gain patterns. Results do reveal some similarity between computed and measured broadside gain and pattern-cuts, but further investigation is required to account for differences in the computational model and prototype.

5.3.2 New One-Layer Design. Computational analysis of the newly developed one-layer structure indicates a marked improvement in performance over the original version. The first noticeable change is that the antenna input impedance has only one strong resonance, see Figure 34. In fact, the resonance is very close to the designed frequency of 3 GHz.

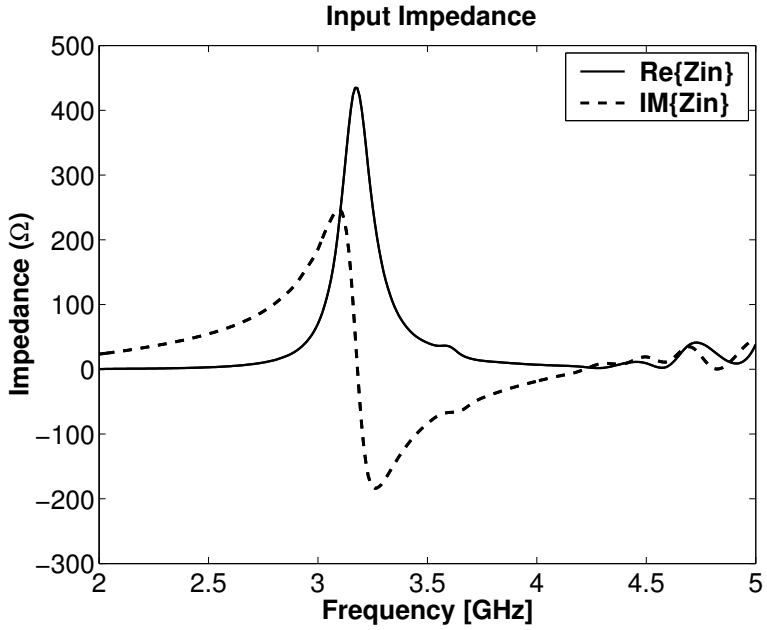

Figure 34 Input impedance of new one-layer HIGP antenna design.

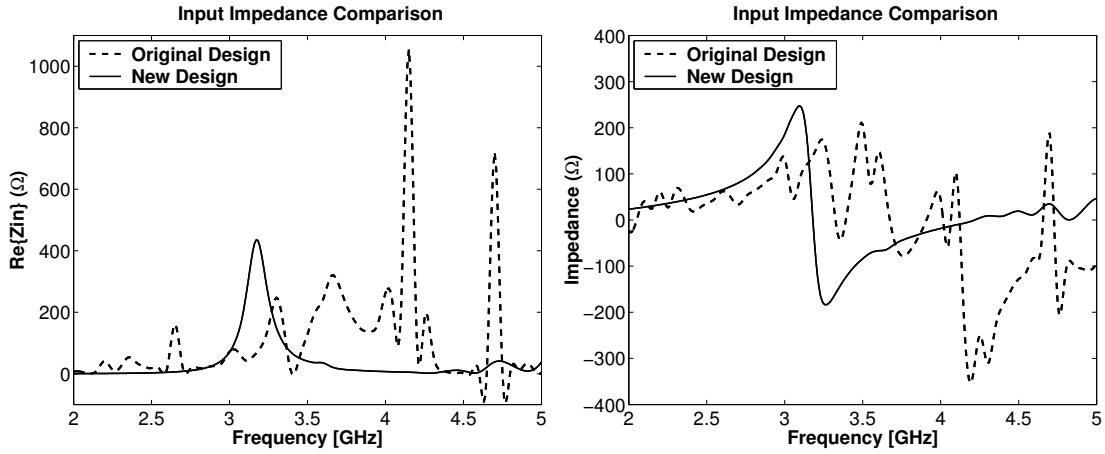

(a) Comparison of Resistance.

(b) Comparison of Reactance.

Figure 35 Computed input impedance for original and new one-layer HIGP antenna deisgns.

Comparing impedance between the two models, the new version has a much lower peak resonance. Figure 35 shows the new design reaches a relatively low peak resistance of 400 Ω compared to the 1200 Ω peak of the original version. The results may be attributed to the closely matched operating band of the new HIGP design with its corresponding bowtie. The lower peak resistance value allows easier matching to a transmission line.

The computed gain and radiation patterns appear promising, see Figure 36. The gain is relatively flat across the 2-5 GHz band. The result poses the question as to whether or not the structure was modeled correctly in Prism. Experimental measurements may provide a valuable second opinion of the gain response. Radiation patterns at 3.0 GHz provide a very good response at the intended center frequency. The patterns are almost identical to those of a bowtie over substrate peak resonance, see Section 5.1. One possible answer for the similarities in patterns may be that the one layer HIGP antenna is only functioning as a bowtie over a substrate–perhaps not influenced by the HIGP. The differences between the original and new one-layer versions may be simply due to the difference in substrate thickness and dielectric constants.

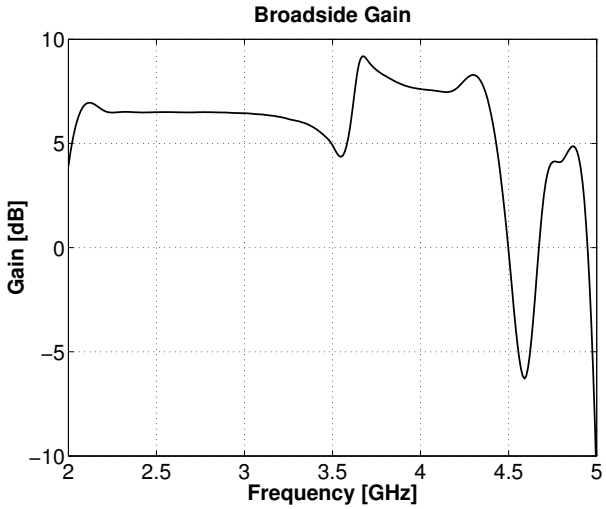

(a) Broadside Gain.

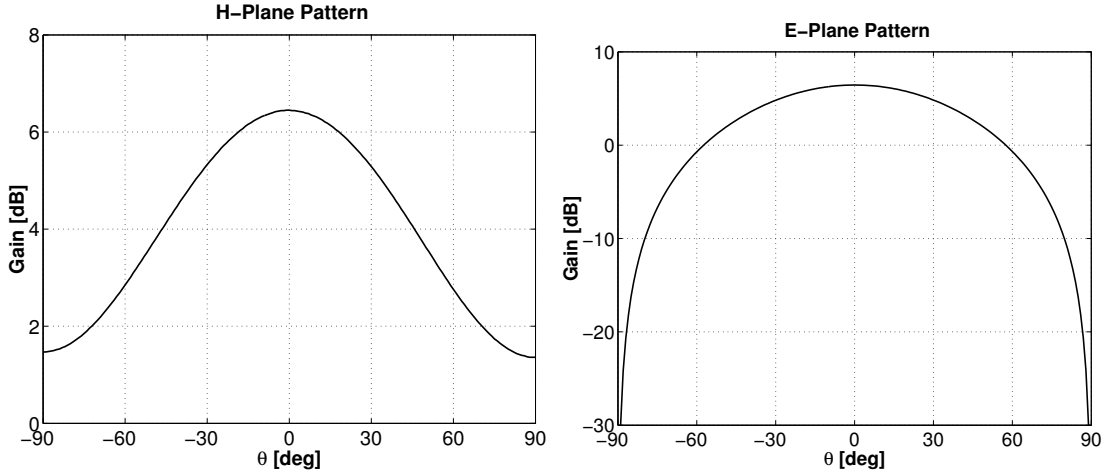

(b) H-plane Radiation Pattern.

(c) E-plane Radiation Pattern.

Figure 36 Broadside gain and radiation patterns of the new one-layer HIGP antenna design.

5.4 Conclusions

Although the new design parameters may lead to a HIGP antenna of the desired resonance and bandwidth, more analysis is required. Initial results using computational methods requires further support in the form of experimental measurements in order to confirm the antenna design. In fact, the one player version may not lend itself to a HIGP design. Analysis of the two-layer HIGP antenna along side of the one-layer version may provide more insight into the HIGP performance.

VI. Conclusion

HIGP based antennas provide a substantial amount of material for a research project. The overall goal of demonstrating a large bandwidth HIGP antenna was not achieved; however, progress was made in areas such as material selection, fabrication, and tying together computational and experimental research for a high bandwidth HIGP antenna.

This research project set out to provide computational and experimental measurements in support of a proposed two-layer HIGP antenna. The predicted bandwidth and resonant frequency of the proposed design are 48% and 3 GHz respectively. Neither computational nor experimental results support the predicted values. In fact, a close examination of the HIGP design equations revealed a mismatch in the HIGP and bowtie antenna structures. The antenna should resonate at 3 GHz, but the HIGP design has a resonant frequency of 1.8 GHz. Even when numerical and experimental results were in agreement, the Wilmhoff design did not demonstrate a bandwidth greater than 16%. On the other hand, a new design was presented which may significantly benefit future research in this area.

A corrected design was developed late in the research. Several lessons learned were applied in its development which ease the fabrication process and reduces computational demand. Computational results of the new design applied to a one-layer version of the HIGP antenna show an improvement over the original design. A two-layer version may even achieve greater performance.

6.1 Recommendations and Future Research

This thesis incorporates many aspects of a design process. As such, an extensive amount of time was devoted to learning new tools and concepts. That comes with the territory. On the other hand, a significant portion of the research was consumed in troubleshooting software. The following sections contain recommendations that could resolve

some of the software issues. In addition, some possible areas of further research are presented along with advice on selecting the operational band of an antenna.

6.1.1 Computational Modeling Process. A golden opportunity exists to develop a better modeling process. Much of this project was devoted to troubleshooting and creating a work-around for software inadequacies. In fact, the modeling process requires several patches to enable input/output interface between software packages. Each patch employs MATLAB® code. The meshing capability of MATLAB® may also be a suitable replacement for SkyMesh2©. Such a change could provide two important advantages. First and foremost, it may provide a better work-around for SkyMesh2 inadequacies related to a multi-layer HIGP structure. Second, it could eliminate some patches and allow consolidating others into a single MATLAB script file. The entire process could be collapsed into just three types of programs: a CAD package, MATLAB®, and Prism. Much of the ground work is already in place.

Another alternative involves an upgrade of WIPL-D. Limitations in the demo version prevent modeling a HIGP surface. The professional version enables modeling of such structures. In addition, an add-on module is available that directly reads in CAD files. Unlike the software involved in the Prism modeling process, a WIPL-D upgrade requires additional funding. A single license for the professional version with a CAD reader comes with a price tag of $8,000.

6.1.2 HIGP Antenna Designs. From an antenna design aspect, analysis of the corrected HIGP antenna is certainly recommended. The one-layer version has already demonstrated good performance and the two-layer version may be even more promising. Continued research may include new efforts such as EBG characterization, RCS analysis, and impedance matching. The structure of the antenna allows impedance matching from either a coaxial or etched balun. Relocation of the bowtie feed points provides another option in changing the antenna input impedance. More challenging problems also exist.

6.1.3 Selection of an Operational Band. Selection of an antenna's operational band requires a few trade-offs. As previously noted, available materials should be considered when deriving values for design parameters. In addition, research involving both computational and experimental analysis combines the shortfalls of each method. Shortfalls of both methods should be taken into account when establishing an operational band.

Computational methods become increasingly taxed with increasing frequency. The demo version of WIPL-D reaches its limit, 700 unknown currents, at about 5 GHz when modeling a relatively small bowtie antenna over a PMC. Even a robust program, such as Prism, can bog down at high frequencies. In order to maintain a consistent accuracy, the physical mesh lengths must decrease proportionally with guided wavelength. At 5 GHz, the HIGP structures in this thesis required solving a few thousand to tens of thousands of unknown fields. Depending on available computing resources, these antennas require run times on the order of days and even weeks. On the other hand, 5 GHz is too low for some experimental measurements.

Much of the available microwave equipment at AFIT is targeted for X-band (8-12 GHz) measurements. The AFIT RCS range has a lower frequency limit of 6.2 GHz due to the horn antennas and RF hardware. The "mini-chamber", AFIT's antenna chamber, has a lower cut-off of 2 GHz. Antenna measurements were also taken at the Air Force Research Laboratory's Radiation and Scattering Compact Antenna Laboratory (RASCAL), but it too prevents measurements below 2 GHz. In addition, in-house network analyzers can measure frequencies from 50 MHz to 20 GHz, but all associated calibration equipment and waveguides are for the X-band measurements. Depending on the selected operational band of the device under test, these hardware limits may or may not limit experimental research.

Bibliography

1. Ali, Muhammod. "Design of a Wideband Microstrip Patch Antenna on a PBG Type Substrate." *Proceedings of the IEEE SoutheastCon 2002*. 48–51. Columbia SC: IEEE Press, 2002.
2. Brown, George H. and O. M. Woodward, Jr. "Experimentally Determined Radiation Characteristics of Conical and Traingular Antennas," *RCA Review*, 425–452 December 1952.
3. Coccioli, Roberto and others. "Aperture-Coupled Patch Antenna on UC-PBG Substrate," *IEEE Trans. Microwave Theory Tech.*, *47*:2123–2130 November 1999.
4. Golla, Keven J. *BroadBand Application of High Impedance Ground Planes*. MS thesis, AFIT/GE/ENG/01M-11, Graduate School of Engineering and Management, Air Force Institute of Technology (AETC), Wright-Patterson AFB OH, March 2001.
5. *RO4000 Series High Frequency Circuit Materials*. Data Sheet RO1.4000. Rogers Corporation, Advanced Circuit Materials Division, Chandler AZ, undated.
6. Knott, Eugene F. and others. *Radar Cross Section* (Second Edition). Norwood MA: Artech House, 1993.
7. Kolundzija, Branko and others. *WIPL-D: Eletromagnetic Modeling of Composite Metallic and Dielectric Structures – Software and User's Manual*. Norwood MA: Artech House, 2000.
8. Neelakanta, Perambur S. *Handbook of Electromagnetic Materials: Monolithic and Composite Versions and Their Applications*. Boca Raton FL: CRC Press, Inc., 1995.
9. Pozar, David M. *Microwave Engineering*. New York: Addison Wesley, 1990.
10. Qian, Yongxi and others. "A Novel Approach for Gain and Bandwidth Enhancement of Patch Antennas." *Proceedings of the RAWCON '98*. 221–224. Colorado Springs CO: IEEE Press, 1998.
11. Rahman, M. and, M.A. Stuchly. "Wide-Band Microstrip Patch Antenna with Planar PBG Structure." *Proceedings of the Antennas and Propagation Society, 2001 IEEE International Symposiuim*. 486–489. Boston: IEEE Press, 2001.
12. Salonen, P. and others. "A Low-Cost 2.45 GHz Photonic Band-Gap Patch Antenna for Wearable Systems." *Proceedings of the IEE 11th International Conference on Antennas and Propagation*. 719–723. London: IEE, 2001.
13. Sandor, Ed, Technical Representative Midwest Region. Telephone interview. Rogers Corporation, Advanced Circuit Materials Division, Chandler AZ, 8 October 2002.
14. Sievenpiper, Daniel F. *High-Impedance Electromagnetic Surfaces*. PhD dissertation, University of California at Los Angeles, Los Angeles CA, 1999.

15. Sievenpiper, Daniel F. and others. "High-Impedance Electromagnetic Surfaces with a Forbidden Frequency Band," *IEEE Trans. Microwave Theory Tech.*, *47*:2059–2074 November 1999.

16. Stutzman, Warren L. and Thiele, Gary A. *Antenna Theory and Design*. New York: John Wiley and Sons, Inc., 1981.

17. Volakis, J. L. and others. *Finite Element Method for Electromagnetics: Antennas, Microwave Circuits, and Scattering Applications.*. IEEE Press, 1998.

18. Wilmhoff, Benjamin R. *A Characterization and Applications of High Impedance Ground Planes with Conformal Antennas*. MS thesis, Michigan State University, Lansing MI, July 2002.

19. Wilmhoff, Benjamin, Graduate Student Michigan State Univeristy. Personal interview. Air Force Institute of Technology, WPAFB OH, 6 August 2002.

20. Yablonovitch, Eli. "Inhibited Spontaneous Emission in Solid-State Physics and Electronics," *Phys. Rev. Lett.*, *58*:2059–2062 May 1987.

Vita

Captain James W. Stewart was born in Montebello, California. He graduated from Northrop High School, Fort Wayne, Indiana in 1983. In September of that same year, he enlisted in the Air Force. After completing Basic Military Training at Lackland AFB, Texas, he was assigned to Keesler AFB, Mississippi, to complete Navigational Aids Technical training. His next assignment was to the 3rd Combat Communications Group at Tinker AFB, Oklahoma, in 1984. From 1988 to 1994, he was assigned to the 2187th Communications Group at Aviano AB, Italy.

In 1995, Captain Stewart entered the Airman Education and Commissioning Program and attended the University of Texas in Austin. He completed a Bachelor of Science Degree in Electrical Engineering and was commissioned a Second Lieutenant in 1998.

Captain Stewart was assigned as a Developmental Electrical Engineer at the National Air Intelligence Center, Production Operations directorate, Acquisitions Support branch, Wright-Patterson AFB, Ohio. There he served as a Threat Support Manager providing technical intelligence support to the Aeronautical Systems Center (ASC) from May 1998 through August 2001.

In August 2001, Captain Stewart entered the Graduate School of Engineering and Management, Air Force Institute of Technology, to begin a Master of Science program in Electrical Engineering. Upon graduation in March 2003, Captain Stewart entered the in-residence PhD program at the Air Force Institute of Technology, Wright-Patterson AFB, Ohio.

REPORT DOCUMENTATION PAGE

Form Approved
OMB No. 074-0188

1. REPORT DATE *(DD-MM-YYYY)*	2. REPORT TYPE	3. DATES COVERED *(From – To)*
25-03-2003	**Master's Thesis**	Aug 2001 – Mar 2003

4. TITLE AND SUBTITLE

ANALYSIS OF BROADBAND HIGP-IMPEDANCE GROUND PLANE ANTENNA DESIGNS

5a. CONTRACT NUMBER

5b. GRANT NUMBER

5c. PROGRAM ELEMENT NUMBER

6. AUTHOR(S)

Stewart, James, W., Captain, USAF

5d. PROJECT NUMBER

5e. TASK NUMBER

5f. WORK UNIT NUMBER

7. PERFORMING ORGANIZATION NAMES(S) AND ADDRESS(S)

Air Force Institute of Technology
Graduate School of Engineering and Management (AFIT/EN)
2950 Hobson Way, Building 640
WPAFB OH 45433-7765

8. PERFORMING ORGANIZATION REPORT NUMBER

AFIT/GE/ENG/03-17

9. SPONSORING/MONITORING AGENCY NAME(S) AND ADDRESS(ES)

Air Force Research Laboratories (AFRL/SNRR), (AFMC)
Attn: Dr. Dan Janning
2241 Avionics Circle
WPAFB OH 45433-7765
DSN: 785-4120 x3544
e-mail: Dan.Janning@wpafb.af.mil

10. SPONSOR/MONITOR'S ACRONYM(S)

11. SPONSOR/MONITOR'S REPORT NUMBER(S)

12. DISTRIBUTION/AVAILABILITY STATEMENT

APPROVED FOR PUBLIC RELEASE; DISTRIBUTION UNLIMITED.

13. SUPPLEMENTARY NOTES

14. ABSTRACT

This research ties together computational and experimental analyzes of two types of high-impedance ground plane (HIGP) antennas. One type of antenna consists of a proposed two-layer design. The structure consists of a bowtie antenna mounted over the surface of a HIGP. The proposed structure was intended to achieve a resonant frequency of 3 GHz and a bandwidth of 48%; however, a design error results in a significant mismatch in operating bands between the antenna and HIGP. Experimental results indicate the structure performs poorly across the entire measured band of 2-5 GHz. A new two-layer design is developed and presented. The new design takes advantage of lessons learned such as designing around material parameters of readily available materials.

Analysis of integrated, or one-layer, HIGP antennas are also presented. The one-layer versions utilize the exact same design parameters as their corresponding two-layer designs; the bowtie radiating element is simply positioned in the plane of, rather than over, the HIGP. Results indicate the design error in the proposed two-layer structure affects the performance of the one-layer version less than the two-layer antenna. A comparison between the original and new integrated HIGP antennas show an improvement in input impedance, but a decrease in bandwidth.

15. SUBJECT TERMS

Broadband antennas, conformal structures, band gaps, electrical impedance, electromagnetic wave reflections, radar reflections, radar cross section surface waves, traveling waves, computer aided design, chemical milling, machine milling.

16. SECURITY CLASSIFICATION OF:			17. LIMITATION OF ABSTRACT	18. NUMBER OF PAGES	19a. NAME OF RESPONSIBLE PERSON
a. REPORT	b. ABSTRACT	c. THIS PAGE			William D. Wood, Maj., USAF
U	U	U	UU	86	19b. TELEPHONE NUMBER *(Include area code)* (937) 255-6565, ext 4280; e-mail: William.Wood@afit.edu

Standard Form 298 (Rev. 8-98)
Prescribed by ANSI Std. Z39-18